CdL Scienza dei Materiali - Fisica delle Nanotecnologie - a.a. 2004/5

Appunti & trasparenze - Parte 5

Versione 3b, Novembre 2004

Francesco Fuso, tel 0502214305, 0502214293 - fuso@df.unipi.it
http://www.df.unipi.it/~fuso/dida

Cenni sulle proprietà ottiche di nanoparticelle; proprietà ottiche di eterostrutture e strutture a confinamento quantico (MQW, QW, QD). Silicio poroso e nanocristalli. Cenni su laser a diodo (eterogiunzione, QD, VCSEL, quantum cascade) e su cristalli fotonici.

4/11/2004 - 9.30+2 ITI M
8/11/2004 - 9.30+2 ITI M

Introduzione

Ottica (nel visible, $\lambda \approx 400–700$ nm)
vs nanotecnologia (dimensioni typ. < 100 nm)
***Apparentemente incompatibili*!!**

Ma:

-comportamento ottico di nanoparticelle e sistemi nanostrutturati *peculiare* per dimensioni sotto lunghezza d'onda
(metalli: scattering di Mie, plasmoni superficiali;
semiconduttori: eccitoni, "atomi artificiali", etc.)

-dispositivi optoelettronici "tradizionali" (LED, laser a diodo) sfruttano film sottili e nanostrutture

-*Nuovi* dispositivi fotonici sfruttano nanotecnologie ("laser nanotecnologici", Organic-LEDs, cristalli fotonici,…)

-*nanofotonica* (es. campo prossimo, vedi SNOM)

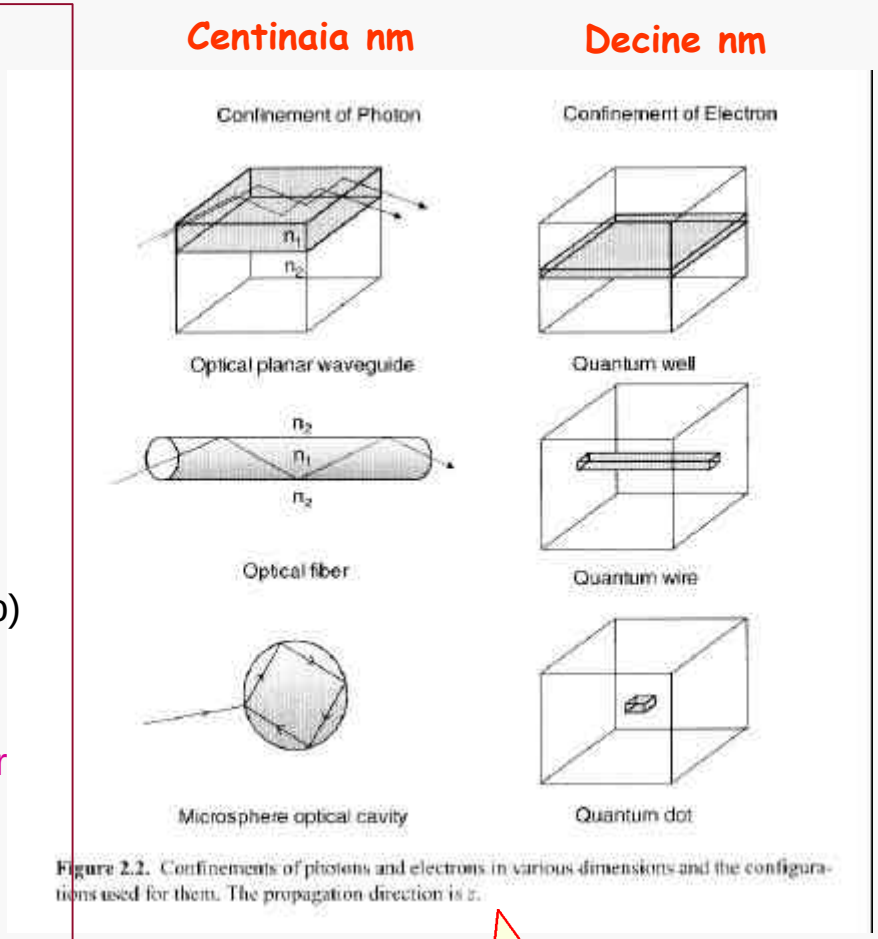

Figure 2.2. Confinements of photons and electrons in various dimensions and the configurations used for them. The propagation direction is z.

Da P.N. Prasad, *Nanophotonics*, Wiley (2004

Proprietà ottiche in nanoparticelle *metalliche* I

Mysterious red color in Lycurgus Cup

Dr. Juen-Kai Wang

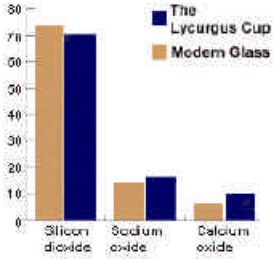

The same composition as modern glass

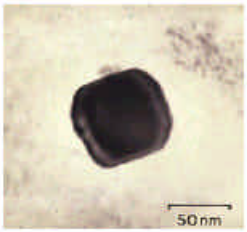

X-ray analysis: 70% Ag + 30% Au

These Ag-Au nanoparticles (~300 ppm) scatter the light, rather in the same way that fine particles in the atmosphere cause a 'red sky at night' effect. They cause the color effects shown by the Cup.

The Lycurgus Cup, Roman (4th century AD), British Museum (www.thebritishmuseum.ac.uk)

See: http://www.ndhu.edu.tw /~nano/93041702.pdf

Gold Building Blocks

Atoms: colorless, 1 Å

Gold clusters: orange, nonmetallic, <1 nm

Gold nanoparticles: 3–30 nm, red, metallic, "transparent"

Gold particles: 30–500 nm metallic, turbid, crimson to blue

Bulk gold film

Figure 1. Gold building blocks, from the atomic to the mesoscopic, and their changing colors.

Au nanoparticles in soluzione

Proprietà ottiche in nanoparticelle *metalliche* II

Grossolanamente:

– effetti di coerenza nella luce scatterata già per $\lambda \sim$ size ;

– effetti di confinamento quantico per size << λ (mean free path in metalli,...)

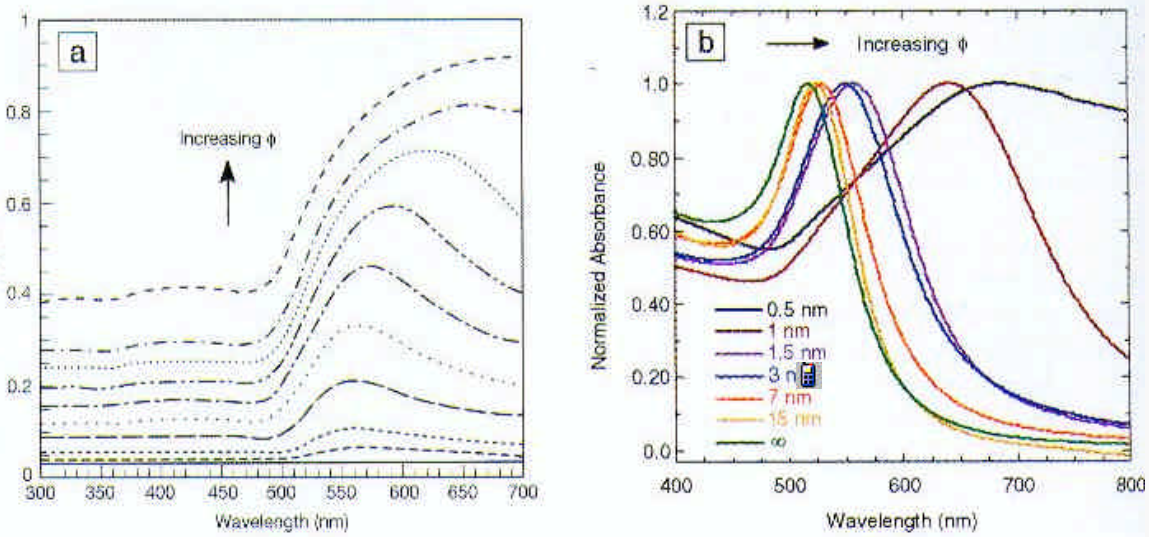

Figure 6. (a) Normalized reflectance spectra for Au@SiO_2 (gold concentrically coated by silica) films as a function of the volume fraction ϕ of Au. From the bottom curve upward, ϕ for each curve, respectively, is 0.01, 0.05, 0.10, 0.20, 0.30, 0.40, 0.50, 0.60, 0.70, and pure Au. (b) The normalized absorbance of a series of Au@SiO_2 films as a function of particle spacing.

Effetti dell'interazione ("colore") dipendono da dimensioni delle nanoparticelle e (da loro spaziatura)

See MRS Bull. 26 (2001)

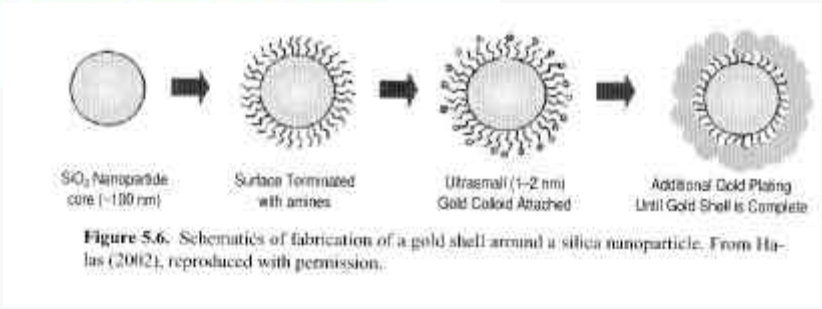

Figure 5.6. Schematics of fabrication of a gold shell around a silica nanoparticle. From Halas (2002), reproduced with permission.

Proprietà ottiche in nanoparticelle *metalliche* III

- For metallic nanoparticles significantly smaller than the wavelength of light, light absorption is within a narrow wavelength range. The wavelength of the absorption peak maximum due to the surface plasmon absorption band is dependent on the size and the shape of the nanocrystals, as well as on the dielectric environment surrounding the particles.
- For extremely small particles (<25 nm for gold), the shift of the surface plasmon band peak position is rather small. However, a broadening of the peak is observed.
- For larger nanoparticles (>25 nm for gold), the surface plasmon peak shows a red shift. Figure 5.1 illustrates these features for a series of gold nanoparticles of different sizes.
- For a nanorod-shaped metallic nanoparticle, the plasmon band splits into two bands corresponding to oscillation of the free electrons along (longitudinal) and perpendicular (transverse) to the long axis of the rod. Figure 5.2 shows this splitting for a gold nanorod.
- The transverse mode resonance is close to that observed for spherical particles, but the longitudinal mode is considerably red-shifted, depending strongly on the aspect ratio, which is the length divided by the width of the rod.

The origin of these shifts is not due to quantum confinement. The quantum confinement does affect the energy spacing of the various levels in the conduction band. However, the quantization, derived from the confinement, affects the conductive properties of the metal and is often used to describe the metal-to-insulator transition occurring as the particle size is reduced from microscopic to nanoscopic size. When the dimensions of the metallic nanoparticles are large, the spacing of levels within the conduction band is significantly less than the thermal energy, kT (k is Boltzmann's constant and T is the temperature in kelvin), and the particle exhibits a metallic behavior. When the nanoparticles approach a size at which the increased energy separation due to the quantum confinement effect (smaller length of the box for the free electron) is more than the thermal energy, an insulating behavior results because of the presence of these discrete levels. However, the energy level separations are still too small to affect the optical properties of metals in the UV to the IR range.

Although a number of theoretical models have been proposed (Kelly et al., 2003), the original classical model of Mie (Born and Wolf, 1998) is often used to

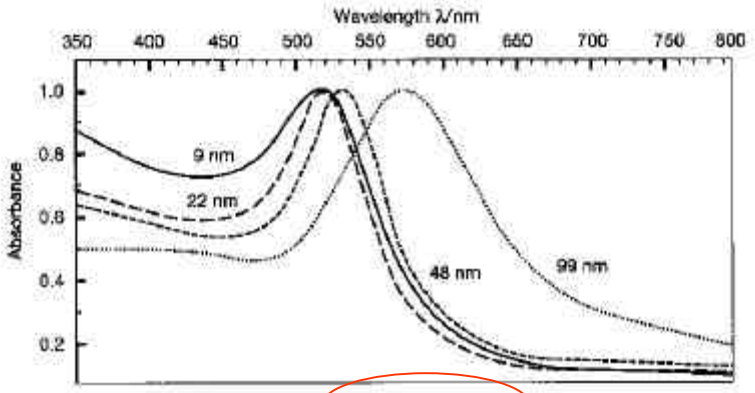

Figure 5.1. Optical absorption spectra of gold nanoparticles of different sizes. From Link and El-Sayed (1999), reproduced with permission.

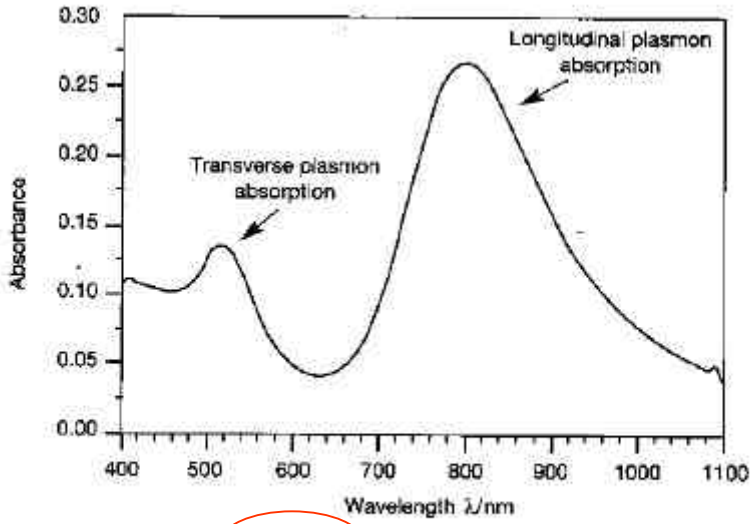

Figure 5.2. Absorbance of gold nanorods. From Link and El-Sayed (1999), reproduced with permission.

Richiami su onde in metalli e frequenza di plasma I

ONDE IN UN MEZZO CONDUTTORE

Fissata la frequenza ω per un' onda e.m. piana di questa frequenza abbiamo: $\dot{\vec{E}} = \frac{\partial \vec{E}}{\partial t} = -i\omega\vec{E}$.

Naturalmente ci siamo riferiti alla notazione complessa dell' onda $\vec{E} = \vec{E}_0 e^{i(\vec{k}\cdot\vec{r}-\omega t)} = E_0 e^{i(kz-\omega t)}\hat{i}$

avendo scelto, per maggiore chiarezza, l' asse z lungo $\vec{k}$ e l' asse x lungo $\vec{E}_0$.

Se l'onda si propaga in un mezzo conduttore di conducibilita' σ, nel materiale sara' presente una densita' di corrente $\vec{j} = \sigma\vec{E}$. L'equazione di Maxwell $rot\vec{H} = \vec{J} + \frac{\partial \vec{D}}{\partial t}$ potra' allora essere riscritta come: $rot\vec{H} = \sigma\vec{E} + \varepsilon_0\varepsilon\dot{\vec{E}} = \sigma\frac{\dot{\vec{E}}}{-i\omega} + \varepsilon_0\varepsilon\dot{\vec{E}}$ e, in definitiva:

$$rot\vec{H} = \varepsilon_0(\varepsilon + i\frac{\sigma}{\varepsilon_0\omega})\dot{\vec{E}}$$

Si vede allora che basta considerare una nuova costante dielettrica per il materiale: alla ε, che e' il contributo delle cariche legate, bisogna aggiungere il contributo delle cariche libere e cioe' quello che nasce dalla conduzione.

Alle frequenze "basse" sia ε che σ sono reali (e positivi). Nei metalli $\sigma \approx 10^8 (\Omega\cdot m)^{-1}$ ed $\varepsilon \approx 1$ per cui, tenendo conto del valore di ε_0, si vede che, fino a frequenze dell' ordine di 10^{14}, si puo' trascurare ε e tenere solo il contributo delle cariche libere $i\frac{\sigma}{\varepsilon_0\omega}$. Inoltre, fino a frequenze dell' ordine di quelle delle microonde, la conducibilita' e' indipendente dalla frequenza ed e' circa uguale alla conducibilita' statica σ_0. Riscrivendo semplicemente quanto gia' trovato nel caso dei dielettrici non magnetizzabili ($\mu \approx 1$ e' un caso generalissimo) si ottiene: $k = \frac{\omega}{c}\sqrt{\varepsilon}$. Essendo $\sqrt{i} = \frac{1+i}{\sqrt{2}}$, si ha

$$\sqrt{\varepsilon} = n + i\beta = \sqrt{\frac{\sigma_0}{\varepsilon_0\omega}}\left(\frac{1+i}{\sqrt{2}}\right).$$

L'ultima espressione mostra che $n = \beta = \sqrt{\frac{\sigma_0}{2\varepsilon_0\omega}}$.

Introducendo il valore di k nell' onda da cui siamo partiti, avremo alla fine

$\vec{E} = E_0 e^{i(kz-\omega t)} = E_0 e^{-\frac{\omega}{c}\beta z} e^{i(\frac{\omega}{c}nz-\omega t)}\hat{i}$ e, da qui, e dalla $rot\vec{E} = -\dot{\vec{B}} \Rightarrow i\vec{k}\wedge\vec{E} = i\omega\vec{B}$,

$$\vec{B} = \frac{n+i\beta}{c}E_0 e^{-\frac{\omega}{c}\beta z} e^{i(\frac{\omega}{c}nz-\omega t)}\hat{j}$$

SIGNIFICATO FISICO DELLA FREQUENZA DI PLASMA.

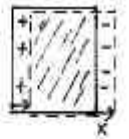

Supponiamo di essere in presenza di un gas completamente ionizzato: $n^+ = n^- = n$ sono le concentrazioni degli ioni positivi e degli elettroni per cui il gas risulta globalmente neutro. Supponiamo anche di far subire agli elettroni uno spostamento x (piccolo) rispetto agli ioni positivi (come avviene nel processo di polarizzazione indotta da un campo elettrico). La situazione e' quella mostrata nella figura: la densita' superficiale delle cariche dei due segni che si e' creata sulle superfici e' nex per cui, nello spazio interno al volume, sara' presente un campo elettrico $E_x = \frac{nex}{\varepsilon_0}$. Ogni elettrone sara' quindi soggetto ad una forza elastica di richiamo

$F_x = -eE_x = -\frac{ne^2x}{\varepsilon_0}$ per cui, una volta lasciato libero, l'elettrone, e con lui tutto il plasma collettivamente, compira' oscillazioni di frequenza propria $\omega_p^2 = \frac{ne^2}{m\varepsilon_0}$ che e' proprio la frequenza di plasma. In presenza di una forza esterna periodica, come quella generata dal campo elettrico di un'onda e.m., ω_p e' la frequenza di risonanza. A questa frequenza l'energia sottratta all'onda sara' particolarmente elevata.

Si noti che la condizione $\omega\tau >> 1$ (e cioe' $\tau >> T$) indica che il periodo T della oscillazione del plasma e' molto piu' piccolo del tempo medio d'urto. Cio' vuol dire che gli elettroni effettueranno un gran numero di oscillazioni forzate di grande ampiezza e, alla fine, cederanno agli ioni tutta l'energia sottratta all' onda, energia che avevano nel frattempo accumulato sotto forma di energia cinetica.

IL MODELLO DI DRUDE DELLA CONDUCIBILITA' ELETTRICA

Correnti stazionarie

In questo modello il moto dell'elettrone dentro un metallo, viene continuamente reso casuale dagli urti con il reticolo entro cui l' elettrone si muove. Se dentro il metallo e' presente un campo elettrico medio $\vec{E}$ l'elettrone, fra due urti successivi, verra' accelerato da questo campo e l'equazione del moto dell'elettrone (massa m, carica $-e$) sara'

$$m\frac{d\vec{v}}{dt} = -e\vec{E}.$$

Al tempo $t = 0$, l' elettrone che aveva subito l'ultimo urto al tempo $-T$, avra' acquistato una velocita' $\vec{v} = \frac{-e\vec{E}}{m}T$. Mediando su tutti gli elettroni la velocita media sara' allora

$$<\vec{v}> = \frac{-e\vec{E}}{m}\tau$$

dove si e' indicato con τ il *tempo medio d' urto* e cioe' il valor medio di T calcolato su tutti gli elettroni.

Se n e' il numero di elettroni liberi per unita' di volume, la densita' di corrente sara'

$$\vec{J} = n(-e)<\vec{v}> = \frac{ne^2\tau}{m}\vec{E}.$$

La conducibilita' statica sara' allora:

$$\sigma_0 = \frac{ne^2\tau}{m}.$$

Nella maggior parte dei metalli $10^{-15}s < \tau < 10^{-14}s$.

Richiami su onde in metalli e frequenza di plasma II

Campi variabili

Se invece di un campo statico e' presente nel metallo un' onda e.m. di frequenza ω, trasurando gli effetti magnetici (in generale molto piccoli), l' equazione per la velocita' media di un elettrone che si trovi nell' origine sara':

$$m\frac{d<\vec{v}>}{dt} = -m\gamma<\vec{v}> - e\vec{E}_0 e^{-i\omega t}.$$

A secondo membro l'ultimo termine e' la forza oscillante che il campo elettrico dell' onda esercita sull' elettrone, mentre il primo termine, una forza di smorzamento viscoso, e' stato introdotto per tener conto degli urti dell' elettrone con il reticolo. Si deve notare che si e' fatta l'ipotesi che il campo elettrico non vari apprezzabilmente su distanze dell' ordine degli spostamenti dell' elettrone durante il suo moto.

Cercando una soluzione in cui $<\vec{v}>$ oscilli con la stessa frequenza ω si trova:

$$<\vec{v}> = \frac{-eE_0 e^{-i\omega t}}{m(\gamma - i\omega)}.$$

Da qui: $$\vec{j} = n(-e)<\vec{v}> = \frac{ne^2\vec{E}}{m(\gamma - i\omega)}$$ per cui

$$\sigma(\omega) = \frac{ne^2}{m(\gamma - i\omega)}.$$

Se si vuole che a frequenza zero, questo risultato riproduca la σ_0 statica, si vede che deve essere $\gamma = \frac{1}{\tau}$.

Si puo' scrivere in definitiva $$\sigma(\omega) = \frac{\sigma_0}{1 - i\omega\tau}.$$

La conducibilita' a basse e ad alte frequenze.

Ricordando che nei metalli $\tau \sim 10^{-14} s$ si vede che, almeno fino alle frequenze delle microonde ($\omega < 10^{11} s^{-1}$), la conducibilita' e' indipendente dalla frequenza ed il suo valore e' uguale alla conducibilita' statica σ_0.

Quando invece $\omega\tau >> 1$, e cioe' per $\omega >> 10^{14} s^{-1}$ (frequenze dell' ultravioletto), si puo' scrivere:

$$\sigma(\omega) = i\frac{\sigma_0}{\omega\tau}.$$

Nei metalli, a queste frequenze, il contributo delle cariche libere alla costante dielettrica diviene allora

$$\frac{i\sigma(\omega)}{\varepsilon_0\omega} = -\frac{\sigma_0}{\varepsilon_0\omega^2\tau} = -\frac{\omega_p^2}{\omega^2}$$

dove abbiamo introdotto un nuovo parametro, la *frequenza di plasma* ω_p definita da

$$\omega_p^2 = \frac{\sigma_0}{\varepsilon_0\tau} = \frac{ne^2}{\varepsilon_0 m}.$$

La frequenza di plasma caratterizza il materiale conduttore; non dipende da τ, ma dipende solamente dalla densita' n dei portatori di carica. Nella maggior parte dei metalli $\omega_p \sim 10^{15} s^{-1}$. Nell'ultravioletto, sempre per i metalli, il contributo alla costante dielettrica delle cariche legate e' molto piccolo , per cui $\varepsilon(\omega)_{legate} \approx 1$. La costante dielettrica complessa e' allora :

$$\varepsilon(\omega) = 1 - \frac{\omega_p^2}{\omega^2}.$$

Per quanto riguarda la propagazione di onde e.m. la frequenza di plasma costituisce allora una frequenza di riferimento precisa. Se la frequenza dell' onda e' $\omega < \omega_p$, la ε e' negativa per cui $\sqrt{\varepsilon}$ sara' immaginaria pura: *la propagazione nel mezzo e' impedita e l' onda, se incide sul metallo, verra' interamente riflessa.*

Se invece $\omega > \omega_p$, $\sqrt{\varepsilon}$ e reale: piu' precisamente $n = \sqrt{(1 - \frac{\omega_p^2}{\omega^2}}$ e $\beta = 0$ per cui *l'onda puo' propagarsi nel mezzo con attenuazione molto piccola* (nelle nostre approssimazioni l' attenuazione e' nulla).

Alle frequenze ottiche, un metallo presenta costante dielettrica ε < 1

Assorbimento dipende da rapporto tra frequenza onda e freq. di plasma

P.L. Braccini, Lezioni di Fisica II
Per ing. TLC (Pisa, 2001)

Scattering di Mie ed effetti collettivi

describe the optical properties of the metal nanoparticles. Often one utilizes a dipole approximation in which the oscillation of conduction electrons (plasmon oscillations), driven by the electromagnetic field of light, produces oscillating dipoles along the field direction where the electrons are driven to the surface of the nanoparticles as shown in Figure 5.3. A more rigorous theory (Kelly et al., 2003) shows that this dipolar-type displacement is applicable to smaller-size particles and gives rise to an extinction coefficient k_{ex} (measure of absorption and scattering strengths collectively) by the following equation (Kreibig and Vollmer, 1995):

$$k_{ex} = \frac{18\pi N V \varepsilon_h^{3/2}}{\lambda} \frac{\varepsilon_2}{[\varepsilon_1 + 2\varepsilon_h]^2 + \varepsilon_2^2} \qquad (5.1)$$

Here λ is the wavelength of light, and ε_h is the dielectric constant of the surrounding medium. The terms ε_1 and ε_2 represent the real and the imaginary parts of the dielectric constant, ε_m, of the metal ($\varepsilon_m = \varepsilon_1 + i\varepsilon_2$) and are dependent on the frequency ω of light. If ε_2 is small or weakly dependent on ω, the absorption maximum corresponding to the resonance condition is produced when $\varepsilon_1 = -2\varepsilon_h$, leading to a vanishing denominator. Hence, a surface plasmon resonance absorption is produced at optical frequency ω at which the resonance condition $\varepsilon_1 = -2\varepsilon_h$ is fulfilled. The size dependence of the surface plasmon resonance comes from the size dependence of the dielectric constant ε of the metal. This is often described as the intrinsic size effect (Link and El-Sayed, 2003). In the case of noble metals such as gold, there are two types of contributions to the dielectric constant of the metal: One is from the inner d electrons, which describes interband transition (from inner d orbitals to the conduction band), and the other is from the free conduction electrons. The latter contribution, described by the Drude model (Born and Wolf, 1998; Kreibig and Vollmer, 1995), is given as

$$\varepsilon_D(\omega) = 1 - \frac{\omega_p^2}{\omega^2 + i\gamma\omega} \qquad (5.2)$$

where ω_p is the plasmon frequency of the bulk metal and γ is the damping constant relating to the width of the plasmon resonance band. It relates to the lifetime associated with the electron scattering from various processes. In the bulk metal, γ has main contributions from electron–electron scattering and electron–phonon scattering, but in small nanoparticles, scattering of electrons from the particle's boundaries (surfaces) becomes important. This scattering produces a damping term γ that is inversely proportional to the particle radius r. This dependence of γ on the particle size introduces the size dependence in $\varepsilon_D(\omega)$ [thus ε_1 in Eq. (5.1)] and, consequently, in the surface plasmon resonance condition.

For larger-size nanoparticles (>25 nm for gold particles), higher-order (such as quadrupolar) charge cloud distortion of conduction electrons becomes important, as shown in Figure 5.4. These contributions induce an even more pronounced shift of the plasmon resonance condition as the particle size increases. This effect for the larger size particle is referred to as the *extrinsic size effect* (Link and El-Sayed, 2003). The position and the shape of the plasmon absorption band also depends on

Scattering by a metal sphere

Dr. Juen-Kai Wang

Induced dipole by the applied field

$$E_{out} = E_0 e_z + \frac{\varepsilon_1 - \varepsilon_2}{\varepsilon_1 + 2\varepsilon_2} \frac{r_1^3}{r^3} E_0 (2\cos\theta e_r + \sin\theta e_\theta)$$

$$\Downarrow$$

$$p = \varepsilon_2 \alpha E_0$$

Effective dipole inside the sphere

$$\alpha = 4\pi r_1^3 \frac{\varepsilon_1 - \varepsilon_2}{\varepsilon_1 + 2\varepsilon_2}$$

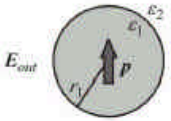

Near-field radiation power from $p(t)$ (near-field scattering cross section)

$$C_{scs}(r) = \int_0^{2\pi} d\theta \int_0^{\pi} d\phi |E|^2 r^2 \sin\theta = \frac{\alpha^2}{6\pi}\left(\frac{3}{r^4} + \frac{k^2}{r^2} + k^4\right)$$

E: the near-field electric field by $p(t)$

$$C_{scs}^{NF} = C_{scs}(r) = \frac{\alpha^2}{6\pi}\left(\frac{3}{r_1^4} + \frac{k^2}{r_1^2} + k^4\right)$$

G. Mie, Ann. Phys. (N.Y.) 25, 377 (1908).

Electron collective motion in metal clusters

Dr. Juen-Kai Wang

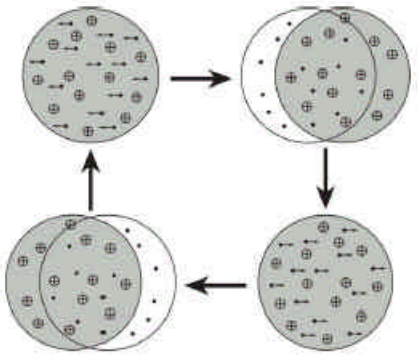

Coherent oscillatory motion

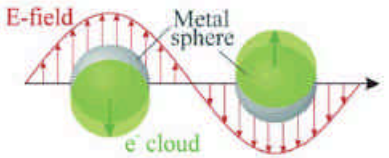

Resonant excitation

Effetti plasmonici superficiali (cenni)

Surface plasmon

Dr. Juen-Kai Wang

$$V_{k\omega}(r,t)=\frac{2\pi\sigma_{k\omega}}{k}e^{-k|z|}e^{j(kx-\omega t)}$$ Surface potential due to surface charge $\sigma_{k\omega}$

$$\varepsilon_1(\omega)E_z\left(z=0^+,\omega\right)=\varepsilon_2(\omega)E_z\left(z=0^-,\omega\right)$$ Boundary condition

$$\because\ E_z\left(z=0^+,\omega\right)=-E_z\left(z=0^-,\omega\right)$$

$$\therefore\ \varepsilon_1(\omega)=-\varepsilon_2(\omega)$$

Plasmon resonance condition

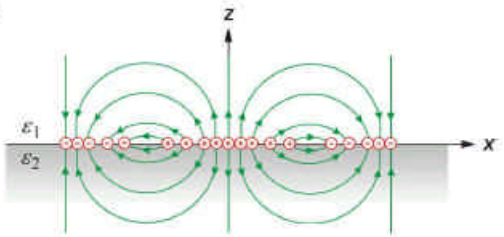

R. H. Ritchie, Phys. Rev. 106, 874 (1957).
Surface Polaritons, edited by V. M. Agranovich and D. L. Mills (North-Holland, Amsterdam, 1982).
M. G. Cottam and D. R. Tilley, Introduction to Surface and Superlattice Excitations (Cambridge University Press, Cambridge, 1989).

$$\because\ k_x^2=\frac{\omega^2}{c^2}\frac{\varepsilon_1\varepsilon_2}{\varepsilon_1+\varepsilon_2}>\varepsilon_1\frac{\omega^2}{c^2}$$

$$\therefore$$ Surface plasmon cannot be excited by a light beam incident in the normal way in medium 1.

Raether-Kretschmann configuration

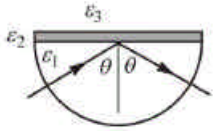

Excitation condition for surface plasmon at the 2/3 interface.

$$k_x=\varepsilon_1^{1/2}\frac{\omega}{c}\sin\theta>\varepsilon_3^{1/2}\frac{\omega}{c}$$

Plasmoni
ed onde evanescenti

Surface plasmon dispersion

Dr. Juen-Kai Wang

Dispersion relation

$$k_x^2=\frac{\omega^2}{c^2}\frac{\varepsilon_1\varepsilon_2}{\varepsilon_1+\varepsilon_2}$$

$$\because\ \varepsilon_1\varepsilon_2<0\ \text{ and }\ k_x^2>0$$

$$\therefore\ \varepsilon_1+\varepsilon_2<0$$

For vacuum-metal surfaces,

$$\varepsilon_1=1\qquad\varepsilon_2=1-\frac{\omega_p^2}{\omega^2}$$

$$\therefore\ 0<\omega<\omega_{sp}\qquad\omega_{sp}^2=\frac{\omega_p^2}{2}$$

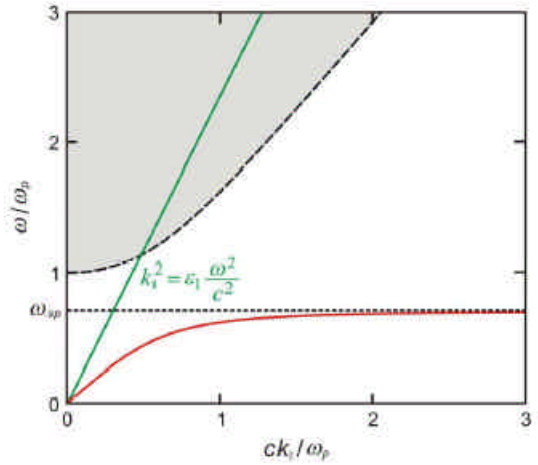

Surface plasmon wave

Dr. Juen-Kai Wang

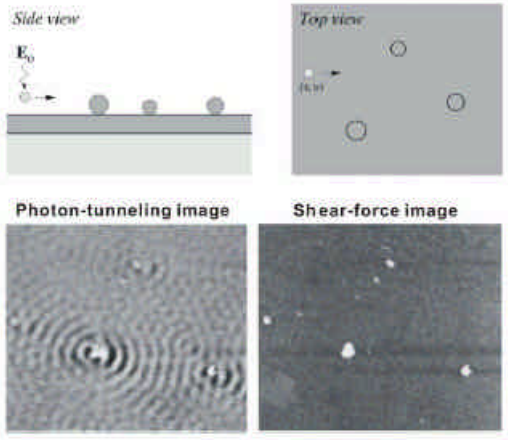

L. Novotny, B. Hecht and D. W. Pohl, J. Appl. Phys. 81, 1798 (1997).

Esempi di preparazione nanoparticelle metalliche

FOTORIDUZIONE

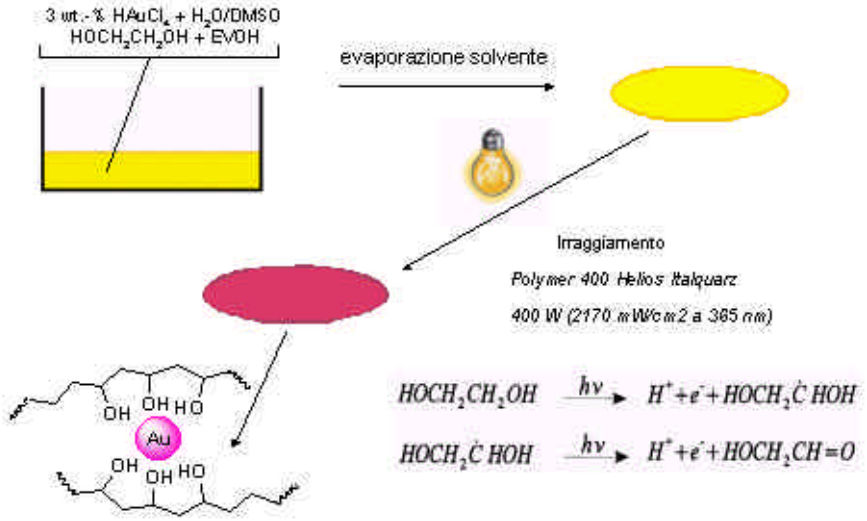

SPETTRO UV RELATIVO A CAMPIONI IRRAGGIATI A TEMPI DIFFERENTI

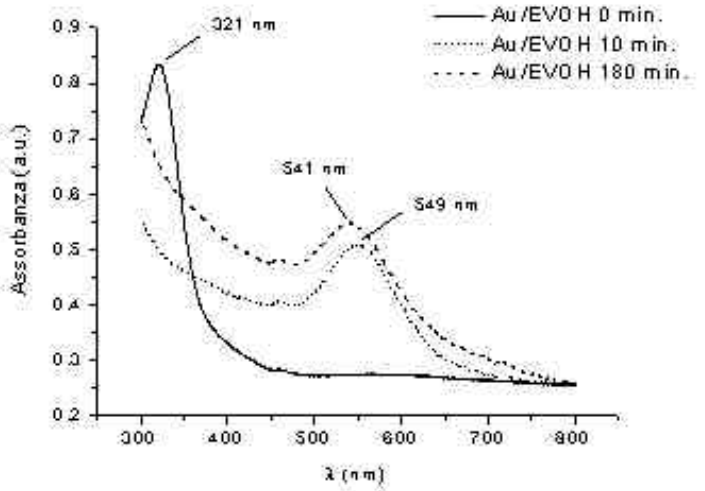

PREPARAZIONE DI NANOPARTICELLE D'ORO STABILIZZATE DA AMMINA O DA TIOLO:

$$m AuCl_4^-{}_{(aq.)} + m N(C_8H_{17})_4^+{}_{(toluene)} \longrightarrow m[N(C_8H_{17})_4^+ AuCl_4^-]_{(toluene)}$$

CON AMMINA

$$m[N(C_8H_{17})_4^+ AuCl_4^-]_{(toluene)} + n(alchilammina)_{(toluene)} + 3me^-_{(aq.)} \longrightarrow$$
$$\longrightarrow 4mCl^-_{(aq.)} + (Au_m)(alchilammina)_{(ad)(toluene)} + x(alchilammina)_{(toluene)}$$
$$+ m[N(C_8H_{17})_4^+]_{(toluene\,aq.)}$$

CON TIOLO

$$m[N(C_8H_{17})_4^+ AuCl_4^-]_{(toluene)} + nC_{12}H_{23}SH_{(toluene)} + 3me^- \longrightarrow$$
$$\longrightarrow 4mCl^-_{(aq.)} + (Au_m)(C_{12}H_{23}SH)_{n(toluene)}$$

Materiale tratto dal seminario di
M. Barnabò, Apr. 2004

Dicroismo per spostamento del plasmone

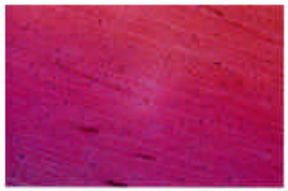

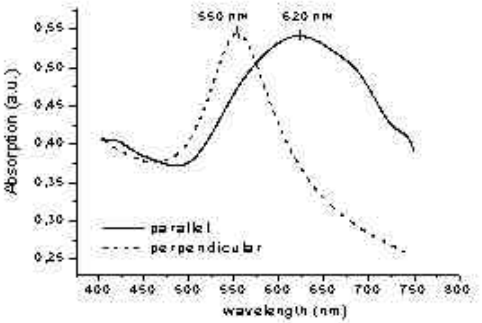

Campioni stretched

Semiconduttori (e dielettrici)

Effetti plasmonici richiedono “elettroni liberi”: effetti tipici per metalli (buoni conduttori)

In semiconduttori? Importanza effetti di confinamento quantico (cariche e radiazione!!)

Storicamente: eterostrutture/superreticoli

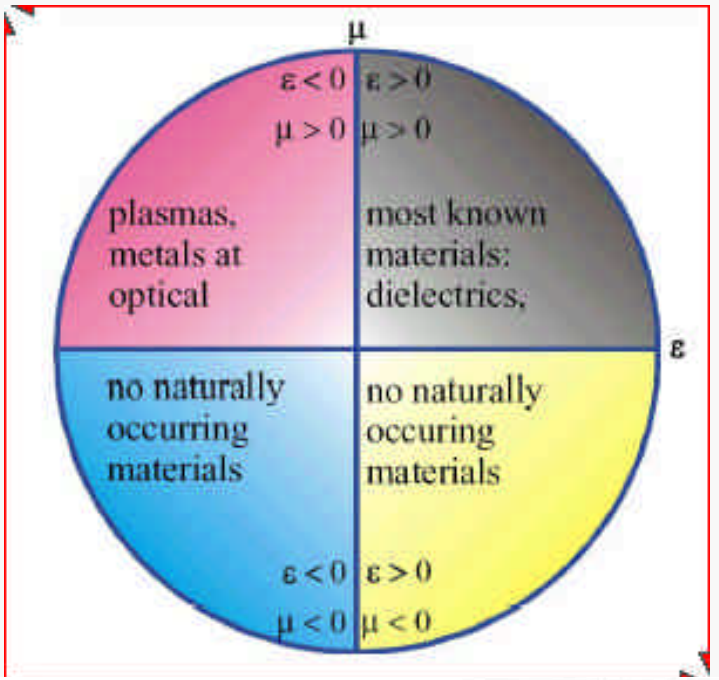

Sistemi disegnati e nanostrutturati “artificialmente”

(Molecular Beam Epitaxy – MBE)

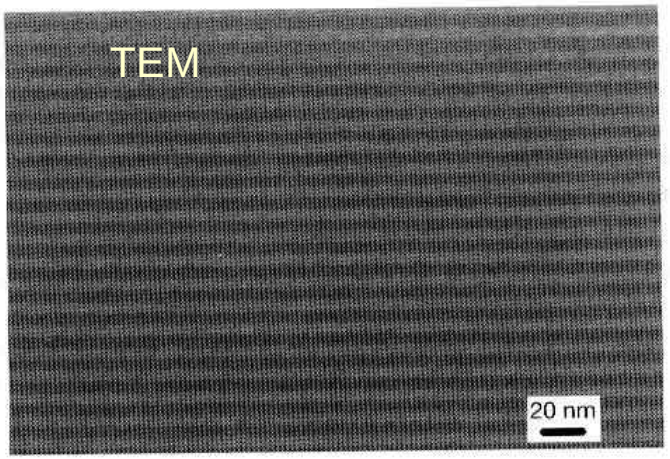

Figure 7. 2. An illustrative example of TEM micrograph of an MBE grown film containing a ZnSe/ZnCdSe superlattice. The bright layers are ZnSe layers, and the dark layers are ZnCdSe layers. Courtesy of Hong Luo, University at Buffalo.

Confinamento quantico: superreticoli e MQW

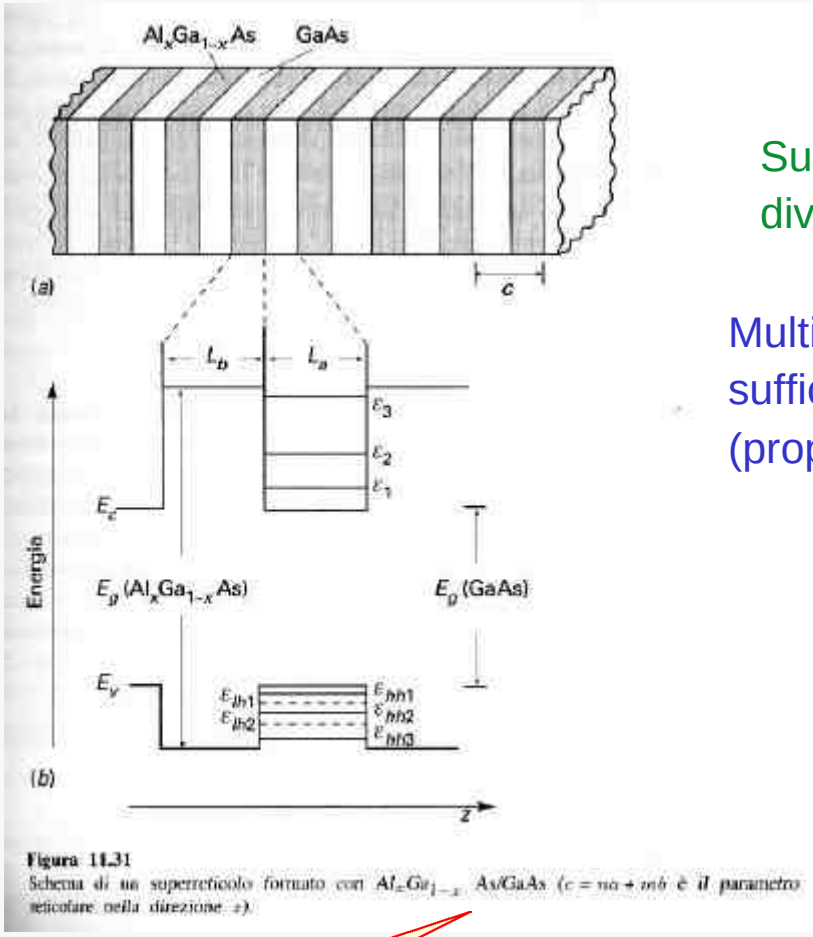

Figura 11.31
Schema di un superreticolo formato con $Al_xGa_{1-x}As$/GaAs ($c = na + mb$ è il parametro reticolare nella direzione z).

Da Bassani Grassano,
Fisica dello Stato Solido,
Boringhieri (2000

Superreticolo: alternanza di strati di semicond. diversi (tip. cresciuti per MBE)

Multiple Quantum Wells: superreticolo con spaziatura sufficiente a impedire tunneling
(proprietà ottiche --> size legata a λ_{rad} , non λ_{dB}!!)

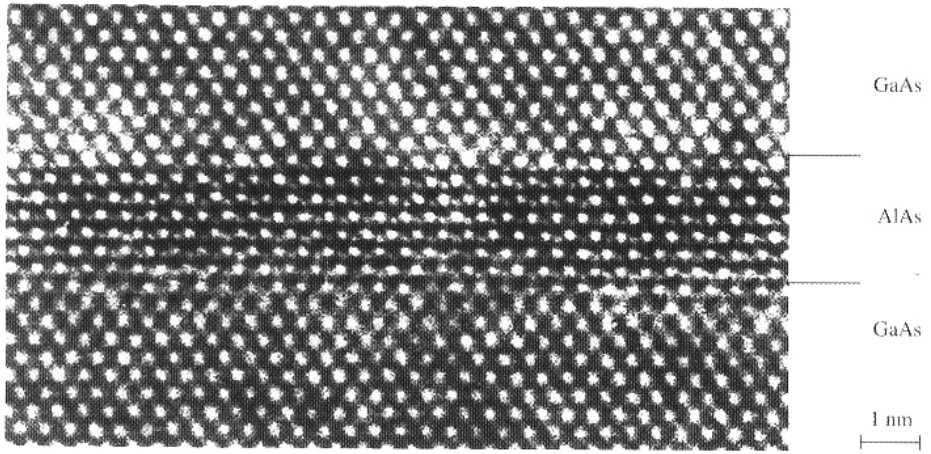

Fig. 9.1. High resolution transmission electron micrograph (TEM) showing a GaAs/AlAs superlattice for a [110] incident beam. (Courtesy of K. Ploog, Paul Drude Institute, Berlin.) In spite of the almost perfect interfaces, try to identify possible Al atoms in Ga sites and vice versa

Crescita di eterostrutture
--> matching reticolare (pseudomorf.)
--> strain/stress
--> critical thickness (e dislocazioni)

Confinamento quantico 2DEG in MQW

Nel blu (~400 nm) oggi si usa GaN

Da Yu and Cardona
Fundamentals of Semicond.
Springer (1996)

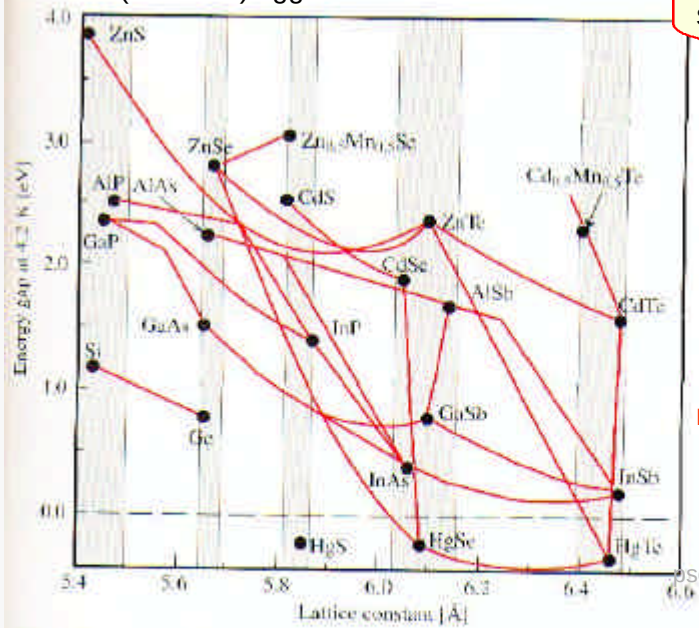

Leghe stabili

Crescita pseudomorfica possibile

Fig. 9.2. A plot of the low temperature energy bandgaps of a number of semiconductors with the diamond and zinc-blende structure versus their lattice constants. The *shaded regions* highlight several families of semiconductors with similar lattice constants. Semiconductors joined by *solid lines* form stable alloys. [Chen A.B., Sher A.: *Semiconductor Alloys* (Plenum, New York 1995) Plate 1]

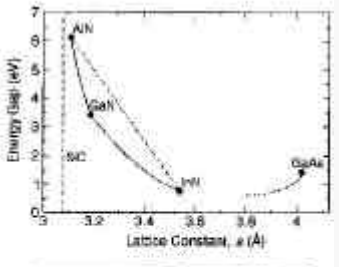

Figure 1. Fundamental bandgap versus basal-plane lattice constant of nitride materials compared with SiC and GaAs. The solid curves represent the ternary mixtures AlN/GaN,[32] GaN/InN,[11] and GaN/GaAs.[19] The dotted curve qualitatively indicates the continuation of the GaNAs gap toward GaN.

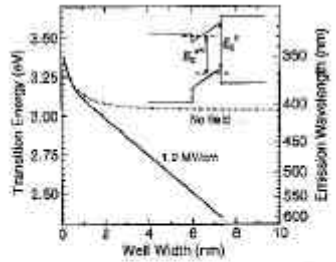

Figure 3. Transition energy of $Ga_{0.8}In_{0.2}N/GaN$ quantum wells versus well width, with and without built-in electric field. The inset shows a schematic view of the band scheme, the effective bandgap E_g^{eff}, and the original bandgap E_g^0.

Emissione nel blu con GaN

See MRS Bull. 27 (July 2002)

Barriere di potenziale in MQW

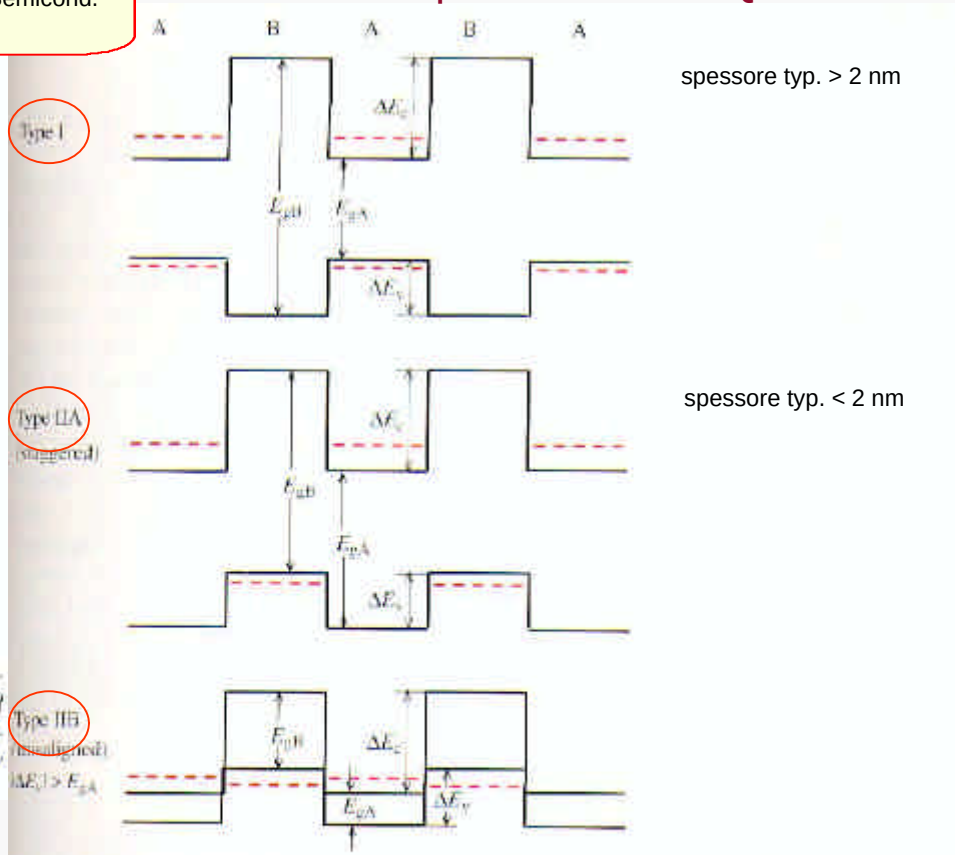

spessore typ. > 2 nm

spessore typ. < 2 nm

Fig. 9.3. Schematic diagrams of three arrangements of the confinement of electrons and holes in MQWs and superlattices formed by two semiconductors A and B with bandgaps E_{gA} and E_{gB}, respectively. In type I samples both the electrons and holes are confined in the same layer A. The energies of the confined particles are represented by *red lines*. In type IIA systems the electrons and holes are confined in different layers. Type IIB samples are a special case of type IIA behavior. They are either small gap semiconductors or semimetals

Es.: A=GaAs (E_{gA} ~ 1.5 eV, lattice 5.653 Å)
B=AlAs (E_{gB} ~ 2.3 eV, lattice 5.62 Å)
opp. B=$Ga_{1-x}Al_xAs$ (con x typ. 0.3)

Buca di potenziale infinita e finita

Da Poole and Owens
Introduction to Nanotechn.
Wiley (2003)

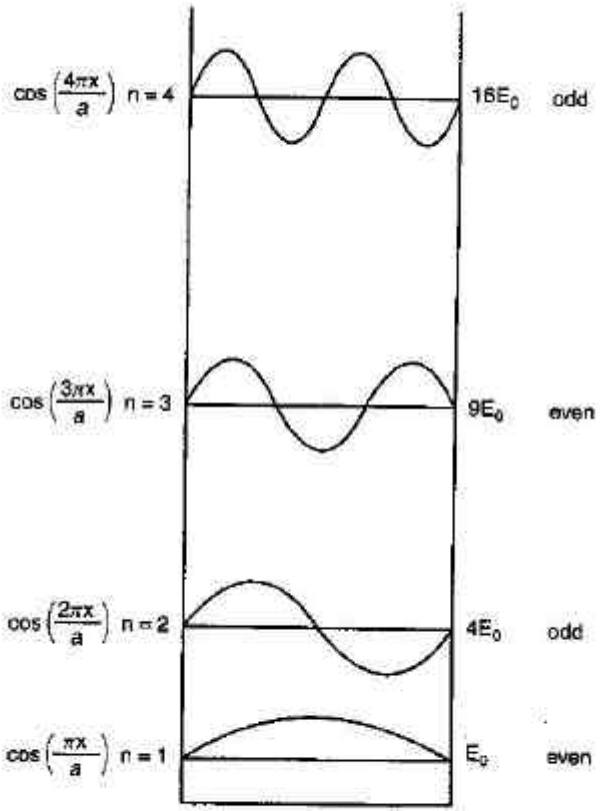

Figure 9.11. Sketch of wavefunctions for the four lowest energy levels ($n = 1$–4) of the one-dimensional infinite square well. For each level the form of the wavefunction is given on the left, and its parity (even or odd) is indicated on the right (From C. P. Poole, Jr., *Handbook of Physics*, Wiley, New York, 1998, p. 289.)

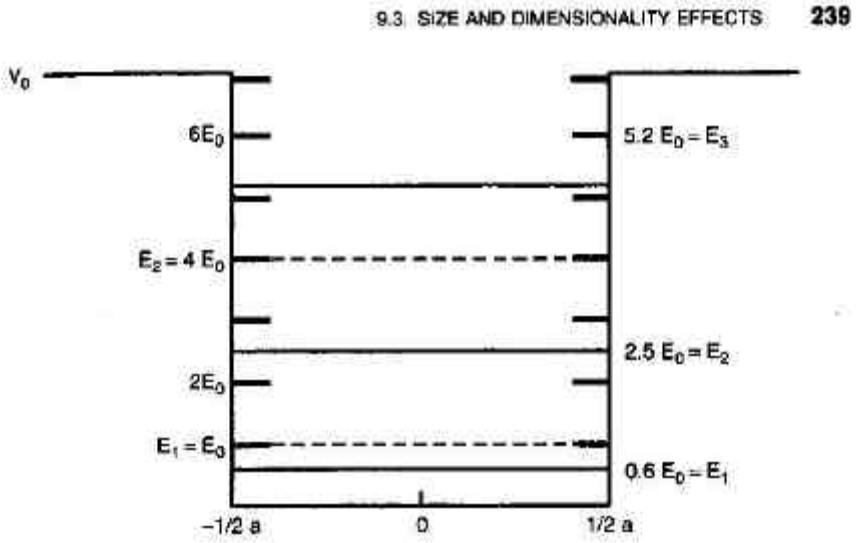

Figure 9.12. Sketch of a one-dimensional square well showing how the energy levels E_n of a finite well (right side, solid horizontal lines) lie below their infinite well counterparts (left side, dashed lines). (From C. P. Poole, Jr., *Handbook of Physics*, Wiley, New York, 1998, p. 285.)

MQW (sistema 2DEG) crea
buche di potenziale unidimensionali
con livelli **discreti** che
dipendono dall'altezza delle pareti
(e dai potenziali di interfaccia)

Livelli e subbands in MQW,

11.9.4 Nanostrutture a dimensionalità ridotta

Pozzi quantici (Q.W. dall'inglese Quantum Wells). Un caso interessante di nanostruttura si presenta quando le barriere sono così spesse che ogni strato tra esse racchiuso si può considerare totalmente isolato dagli altri. In tal caso la simmetria traslazionale è completamente interrotta nella direzione z, dove la differenza tra E_{gA} ed E_{gB} introduce un potenziale di confinamento V_0. Il sistema presenta allora stati discreti nella direzione z, in corrispondenza ad ognuno dei quali si ha una banda bidimensionale in k_x, k_y (sottobanda).

Sviluppando la soluzione generale in funzioni di Bloch dei cristalli perfetti ed utilizzando l'approssimazione di considerare solo gli stati al massimo ed al minimo della banda, con un procedimento analogo a quello usato per i campi magnetici e le impurezze, si giunge alla seguente equazione per la funzione di inviluppo:

eq. di Schrödinger

$$\left[-\frac{\hbar^2}{2}\left(\frac{1}{m_x^*}\frac{\partial^2}{\partial x^2}+\frac{1}{m_y^*}\frac{\partial^2}{\partial y^2}+\frac{1}{m_z^*}\frac{\partial^2}{\partial z^2}\right)-eV_0(z)\right]\psi(r)=E\psi(r). \qquad (11.91)$$

Cerchiamo una soluzione del tipo:

onde piane lungo x ed y

$$\psi(r)=\varphi_n(z)e^{ik_x x+ik_y y}=\varphi_n(z)e^{i\vec{k}_\parallel\cdot\vec{r}}. \qquad (11.92)$$

Sostituendo la (11.92) nella (11.91) si possono separare due equazioni indipendenti:

$$\left[-\frac{\hbar^2}{2m_z^*}\frac{\partial^2}{\partial z^2}-eV_0(z)\right]\varphi_n(z)=E_n(0)\varphi_n(z) \qquad (11.93)$$

$$\left(-\frac{\hbar^2}{2m_x^*}\frac{\partial^2}{\partial x^2}-\frac{\hbar^2}{2m_y^*}\frac{\partial^2}{\partial y^2}\right)e^{i(k_x x+k_y y)}=E_{xy}e^{i(k_x x+k_y y)} \qquad (11.94)$$

La soluzione della (11.94) ha come autovalori quelli di una particella libera di muoversi nel piano xy:

$$E_{xy}=\frac{\hbar^2}{2m_x^*}k_x^2+\frac{\hbar^2}{2m_y^*}k_y^2=\frac{\hbar^2}{2m_\parallel^*}k_\parallel^2. \qquad (11.95)$$

La soluzione della (11.93) dipende dalla forma di $V(z)$. Nella ipotesi semplificatrice di una buca di larghezza L_w a pareti infinite, si ottiene:

buca infinita

$$E_n(0)=\frac{\hbar^2\pi^2}{2m_z^*}\frac{n^2}{L_w^2}, \qquad (11.96)$$

ove $n=1,2,\ldots$

L'energia totale è dunque:

$$E_n(k_\parallel)=\frac{\hbar^2k_\parallel^2}{2m_\parallel^*}+E_n(0). \qquad (11.97)$$

subbands

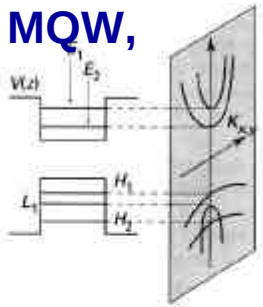

Stati elettronici dispersione $\vec{K}$

DOS 2D

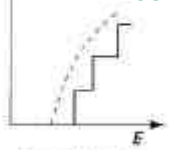

Densità di stati

Figura 11.33
Schema di un pozzo quantico (Q.W.) con indicazione dei livelli da confinamento degli elettroni ($E_1, E_2 \ldots$) e delle buche (pesanti H_1 e H_2, leggere L_1). Sono pure indicate le sottobande (k_x, k_y) corrispondenti ad ogni livello, e la densità di stati (a gradino) in corrispondenza ad ogni soglia di eccitazione.

Da Bassani Grassano, Fisica dello Stato Solido, Boringhieri (2000

Come si vede in fig. 11.33a, essa ha forma parabolica in dipendenza da k_x e k_y e queste parabole sono separate fra loro della quantità $E_n(0)$. Le parabole $E(k)$ in due dimensioni sono chiamate sottobande ed hanno densità di stati costante come indicato nel cap. 8 e mostrato in fig. 11.33b.

Considerando il potenziale finito, si ottiene una correzione alle espressioni precedenti dalle opportune condizioni al contorno. Il calcolo per gli stati di buca è più complesso per la degenerazione della banda di valenza, che richiede un calcolo con l'operatore $E_{ij}(\vec{k})$ ottenuto dalla matrice di Luttinger. L'effetto principale è ottenibile dalla simmetria ridotta, che richiede la separazione degli stati di massa pesante da quelli di massa leggera E_{1hh}, E_{1lh}, E_{2hh}, ... ecc.

heavy and light holes

In corrispondenza a tutti gli stati discreti si ottengono "sottobande" $E_n(k_x, k_y)$, di natura bidimensionale. A titolo di esempio riportiamo in fig. 11.34 sottobande calcolate di elettroni e buche per il caso più comune di pozzi quantici di GaAs, confinati da $Ga_{1-x}Al_xAs$ (con $x = 0.3$).

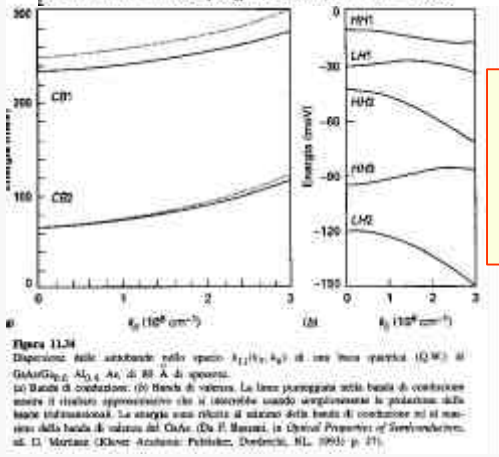

Figura 11.34
Dispersione delle sottobande nello spazio $k_\parallel(k_x, k_y)$ di una buca quantica (Q.W.) di $GaAs/Ga_{0.7}Al_{0.3}As$ di 80 Å di spessore.
(a) Bande di conduzione; (b) Bande di valenza. La linea punteggiata nella banda di conduzione mostra il risultato approssimativo che si ottiene usando semplicemente la massa della buca tridimensionale. La energia zero riferita al minimo della banda di conduzione nel materiale della banda di valenza del GaAs. (Da F. Bassani, in *Optical Properties of Semiconductors*, ed. D. Martinez (Elsevier Academic Publishers, Dordrecht, NL, 1993) p. 37).

Sistema discreto
di sottobande
(con rimozione deg.)

Nanostrutture 1D e 0D (quantum wires and dots)

Da Bassani Grassano,
Fisica dello Stato Solido,
Boringhieri (2000

Fili quantici. In questo caso, mediante tecniche opportune di eliminazione di sostanze o di creazione di barriere nei piani si può ottenere confinamento laterale anche nella direzione y, oltre che nella direzione z. Due pozzi quantici che si incrociano producono anch'essi un tale effetto.

In questo caso la simmetria traslazionale è preservata soltanto nella direzione x. Il nome di "fili quantici" è dato a tali nanostrutture, perché le sottobande sono monodimensionali $E_{n,m}(k_x)$, e il confinamento ha luogo su una superficie, che in prima approssimazione può essere considerata cilindrica.

Nei fili quantici il vantaggio è di avere conducibilità elettrica unidimensionale e stati di radiazione che si propagano soltanto nella direzione x. L'importanza per i laser è evidente, perché in tal caso la collimazione della radiazione è ottenuta per effetto geometrico.

Punti quantici (Q.D.). La nanostruttura più difficile da ottenere, ma anche la più complessa per i suoi effetti sulle proprietà ottiche e di trasporto, è quella in cui il confinamento del materiale a "gap" inferiore avviene in tutte e tre le direzioni dello spazio. Dal punto di vista della simmetria di traslazione si può allora dire che la struttura è a dimensionalità zero, e per questo viene chiamata "punto quantico" (Q.D. dall'inglese Quantum Dot). I livelli di energia per gli elettroni e per le buche sono solo livelli discreti, risultanti dal confinamento. Si può ottenere una prima grossolana approssimazione per gli elettroni dal calcolo quantistico degli stati della buca cubica a pareti infinite di lato L,

$$E_{n_x,n_y,n_z} = E_g + \frac{\pi^2\hbar^2}{2m^*L^2}(n_x^2 + n_y^2 + n_z^2), \qquad (11.92)$$

con $(n_x, n_y, n_z = 1, 2, \ldots)$. Si ottiene un simile risultato per le buche, con la separazione tra stati di massa pesante e di massa leggera dovuti al confinamento. Il calcolo preciso, con potenziale finito, richiede anche in questo caso l'uso delle condizioni di continuità al contorno e lo sviluppo della matrice di Luttinger per le buche.

Ridotta dimensionalità
--> engineered level scheme
(tip. E nel range ottico)

Soluzione colloidale di nanocrist.

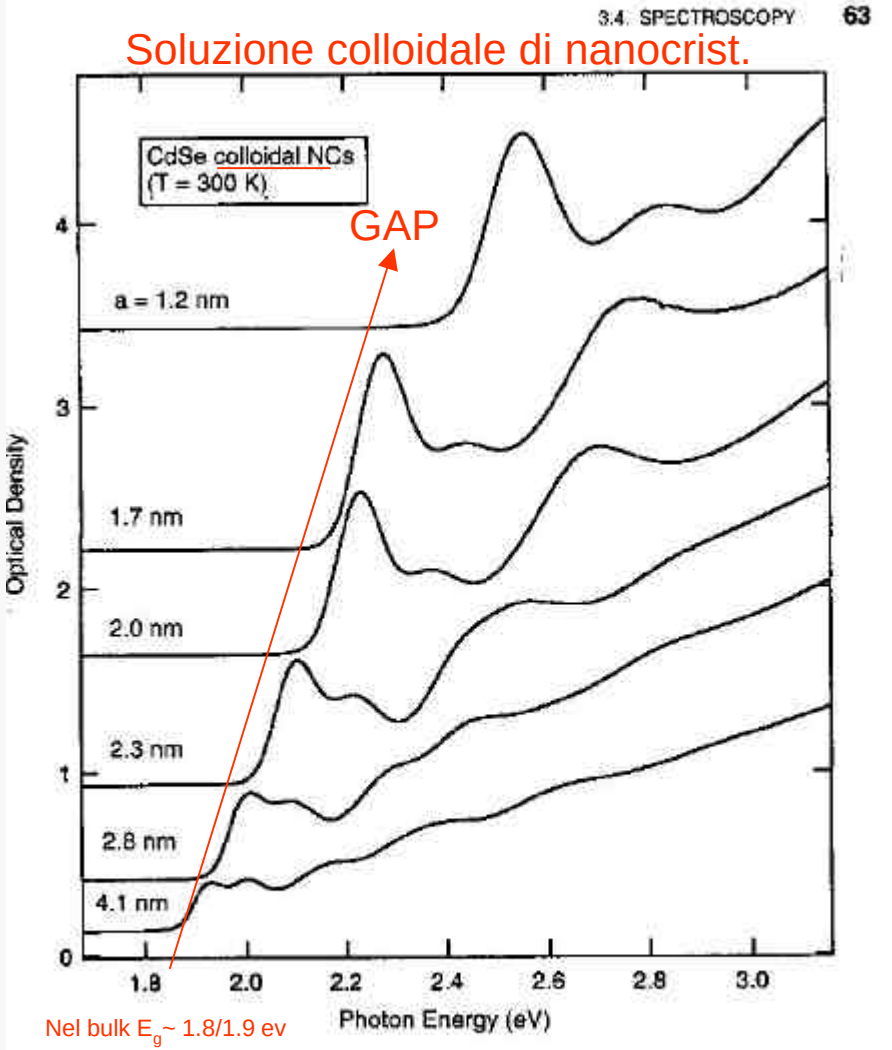

Nel bulk E_g~ 1.8/1.9 ev

ure 3.27. Room-temperature optical absorption spectra for CdSe colloidal nanocrystals
Cs) with mean radii in the range from 1.2 to 4.1 nm. [From V. I. Klimov, in Naiwa (2000),
l. 4, Chapter 7, p. 464.]

C.P.Poole F.J.Owens
Introd. to Nanotechnology
(Wiley, 2003)

Cenni sugli eccitoni

Coppie elettrone-buca (ad es., generate via photon absorption) possono dare origine a sistemi legati (per forza Coulomb.): eccitoni

Il calcolo dell'energia di legame degli eccitoni può essere effettuato in modo analogo a quello delle impurezze nei semiconduttori se le bande di valenza e di conduzione sono sferiche e non degeneri. Analogamente a quanto visto nel cap. 11, si ricava che i livelli idrogenoidi (riferiti alla cima della banda di valenza) hanno energie date da:

atomi artificiali con livelli idrogenoidi

$$E_n = E_g - \frac{\mu e^4}{2\hbar^2 \varepsilon^2} \frac{1}{n^2}, \qquad (12.107)$$

ove n è il numero quantico principale, ε la costante dielettrica, e μ la massa ridotta del complesso elettrone-buca

$$\frac{1}{\mu} = \frac{1}{m_e^*} + \frac{1}{m_h^*}. \qquad (12.108)$$

Nei semiconduttori abbiamo visto che $\varepsilon \simeq 10$ e $\mu \simeq 0.5 m_e$, per cui l'energia di legame degli eccitoni sarà dell'ordine di qualche decina di meV. A causa della grande costante dielettrica l'eccitone è dunque debolmente legato e la distanza media elettrone-buca è dell'ordine di decine di distanze reticolari. Un eccitone con queste caratteristiche è chiamato eccitone di Wannier-Mott, e ne discuteremo

In sistemi a conf. quant. si ha alta probabilità di avere eccitoni (per overlap f.ni d'onda *e-h*)

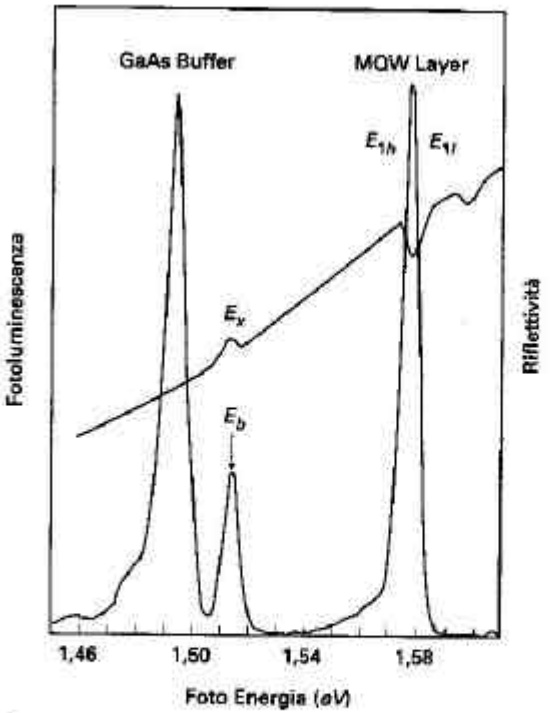

Figura 12.28
Fluorescenza eccitonica da un pozzo quantico (Q.W.) $GaAs/Ga_{1-x}Al_xAs$ e dal substrato GaAs a 12 K. E_b indica la posizione dell'eccitone nel substrato, E_{1h} ed E_{1l} gli eccitoni di buca pesante e di buca leggera nel Q.W. Per confronto è riportata anche la riflettività. Il picco di buca leggera compare soltanto ad alte temperature in fluorescenza, mentre è visibile in riflettività. (Da Y. Chen, R. Cingolani, L.C. Andreani, F. Bassani e J. Massies, Il Nuovo Cimento **D10**, 847 (1988)).

Ricombinazione eccitoni --> fotoni

⇩

elevata probabilità di ricombinazione (alta efficienza quant.)

Esempio di effetti di eccitone in QD

InP islands grown on and capped with InGaP
(fabbricate via MetallOrganic VaporPhaseEpitaxy)

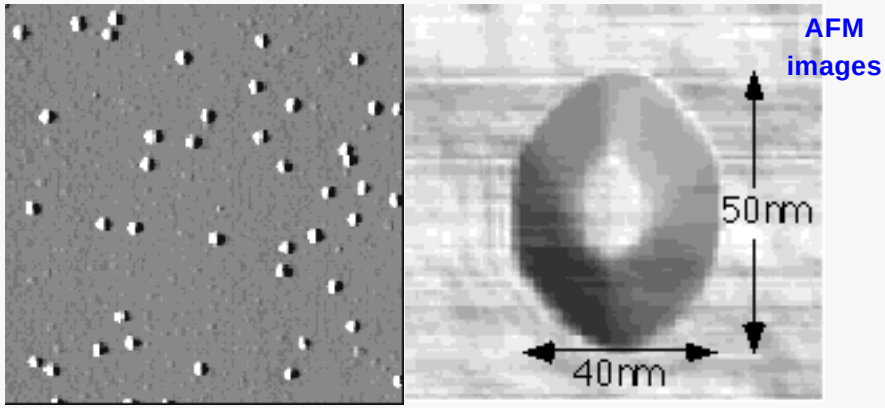

Ogni isola contiene nanocristalli (QD!!!)

Nanocristalli isolati prodotti per MO-VPE

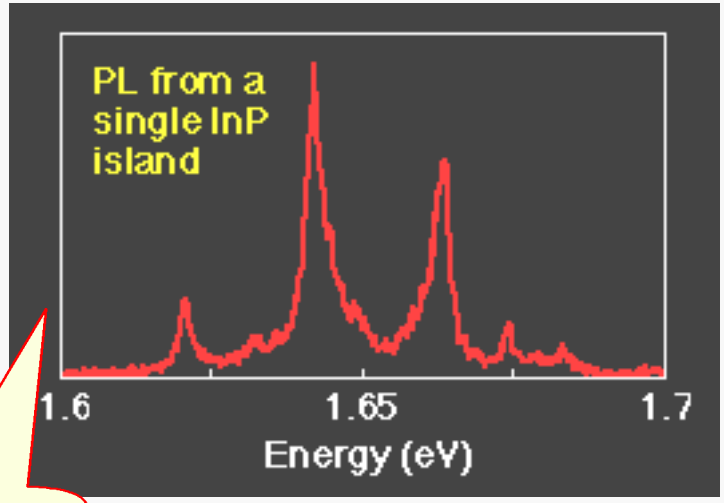

See Hessmann et al.
APL 68 (1996)

Nel bulk E_g~ 1.5 ev

Signatures dell'effetto eccitonico in nanoparticles (ancorate):
- aumento efficienza (PL da *singola* isola)
- features spettrali con rimozione degenerazione (visibili a **temp. ambiente**)

QD isolati e in colloidi I

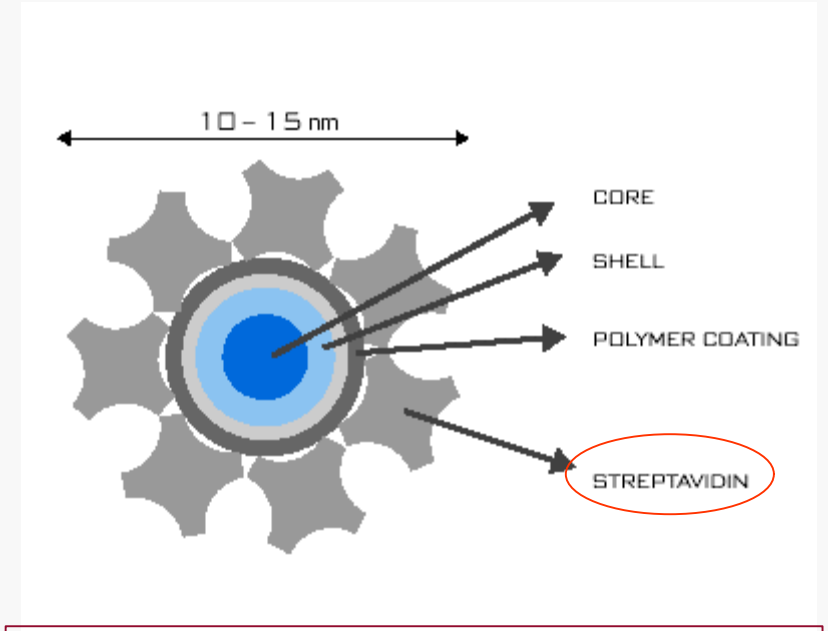

Preparazione:
Core (CdSe)
$Cd(CH_3)_2$ e Se in TBP o TOP
reazione a 360°C e raffreddata 290°C, temp ambiente
controllo crescita tramite spettro di assorbimento
Shell (ZnS)
$(TMS)_2S$ e $Zn(Et)_2$ in TOP
reazione a 190°C
controllo crescita spettroscopia UV-Vis e fotoluminscenza

Materiale tratto dal seminario di Marco Cirillo, Apr. 2004

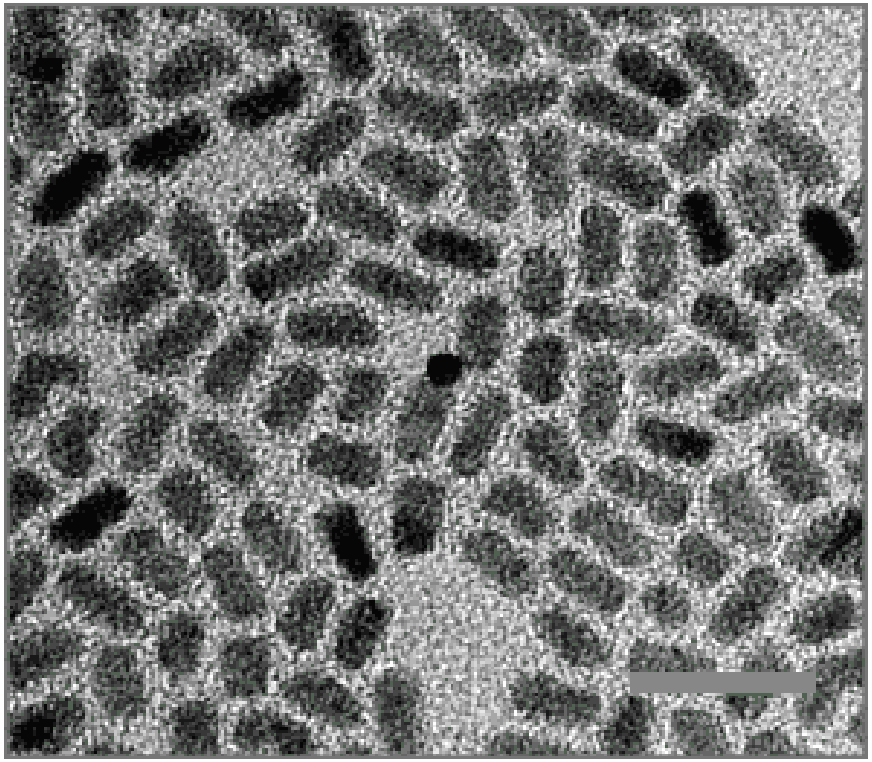

Immagine TEM nanocristalli core-shelll'ingrandimento è 200,000 e la barra è di 20 nm.

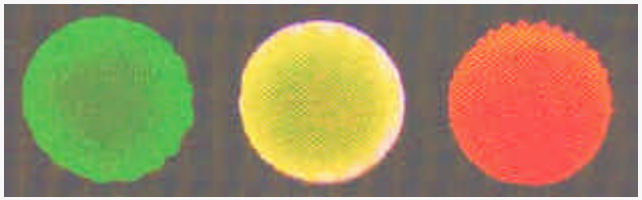

QD isolati e in colloidi II

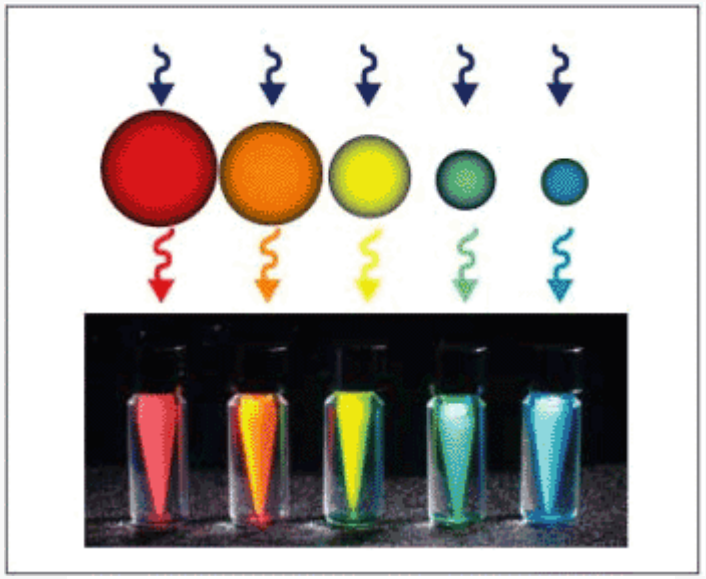

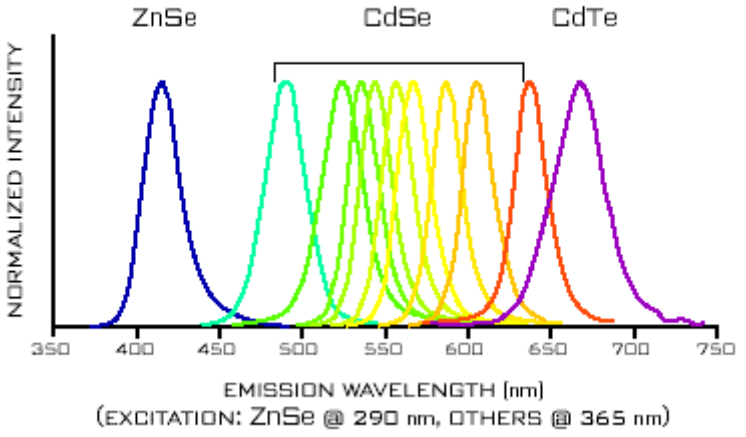

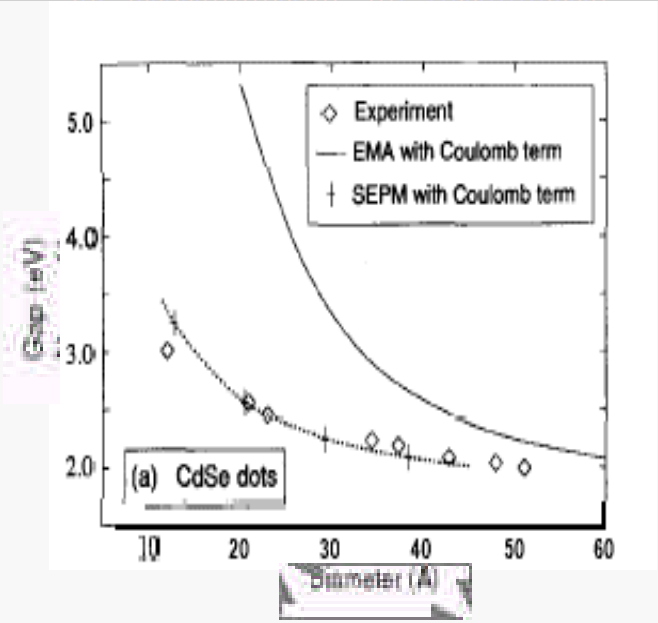

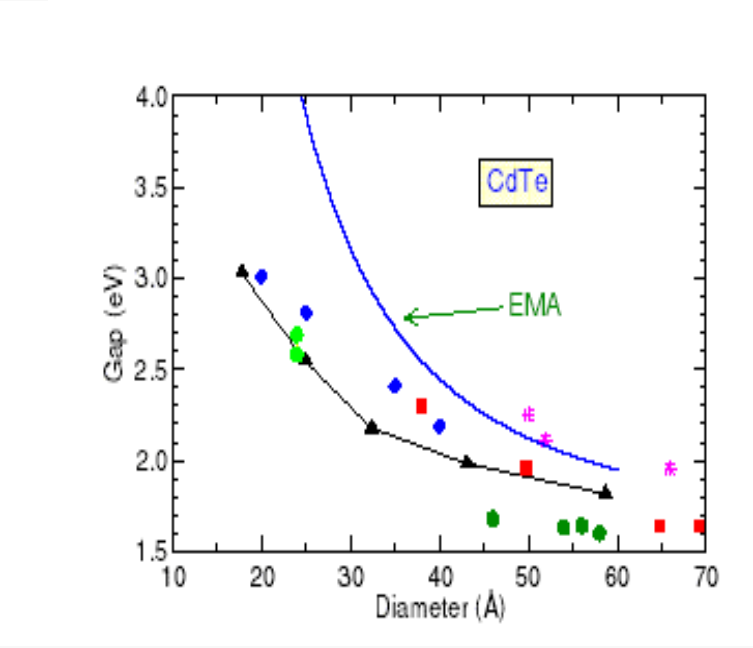

QD come marcatori in biologia

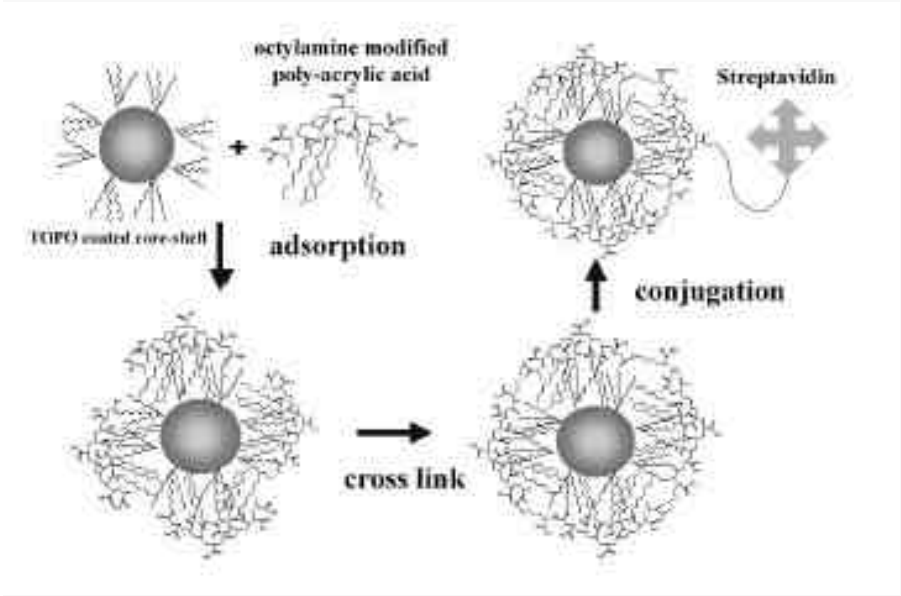

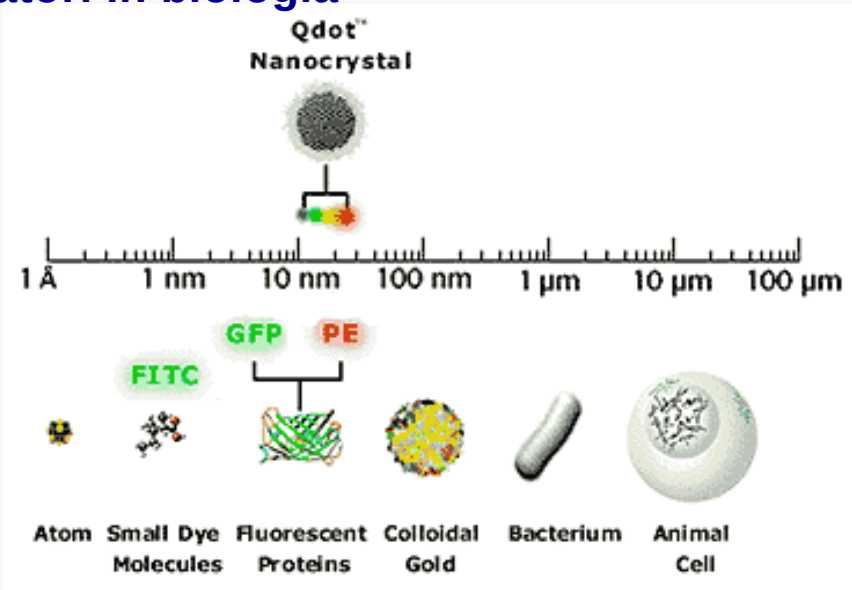

Quantum Dots preferiti a coloranti molecolari per:

-Maggiore efficienza quantica;
-Maggiore “compatibilità”;
-Buona “flessibilità”

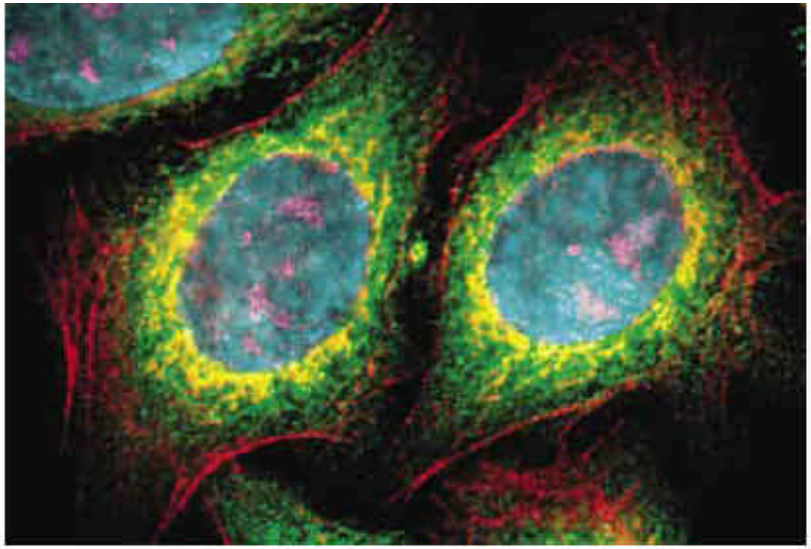

Silicio poroso (e nanocristalli di Si)

Nanocristalli (nc-Si) di forma filamentare
creati nel bulk attraverso etching elettrochimico
(in soluzione di HF) di silicio cristallino (c-Si)

Electropolishing (alta corrente):

$$Si + 6F^- \xrightarrow{+4e} SiF_6^{2-}$$

Porizzazione (H evolve in sup.):

$$Si + 6F^- + 2H^+ \xrightarrow{+2e} SiF_6^{2-} + H_2$$

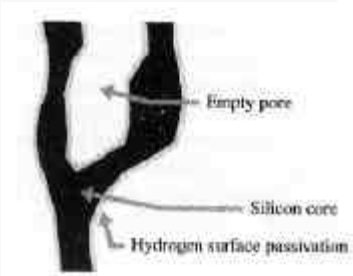

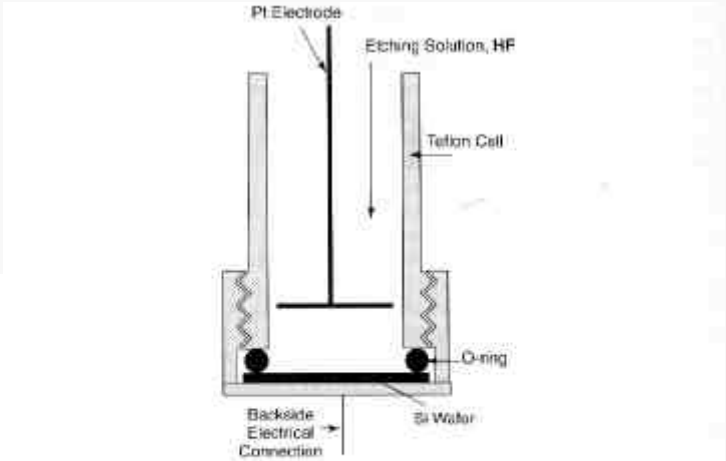

igure 6.21. A cell for etching a silicon wafer in a hydrogen fluoride (HF) solution in order to troduce pores. (With permission from D. F. Thomas et al., in *Handbook of Nanostructured laterials and Nanotechnology*, H. S. Nalwa, ed., Academic Press, San Diego, 2000, Vol. 4, hapter 3, p. 173.)

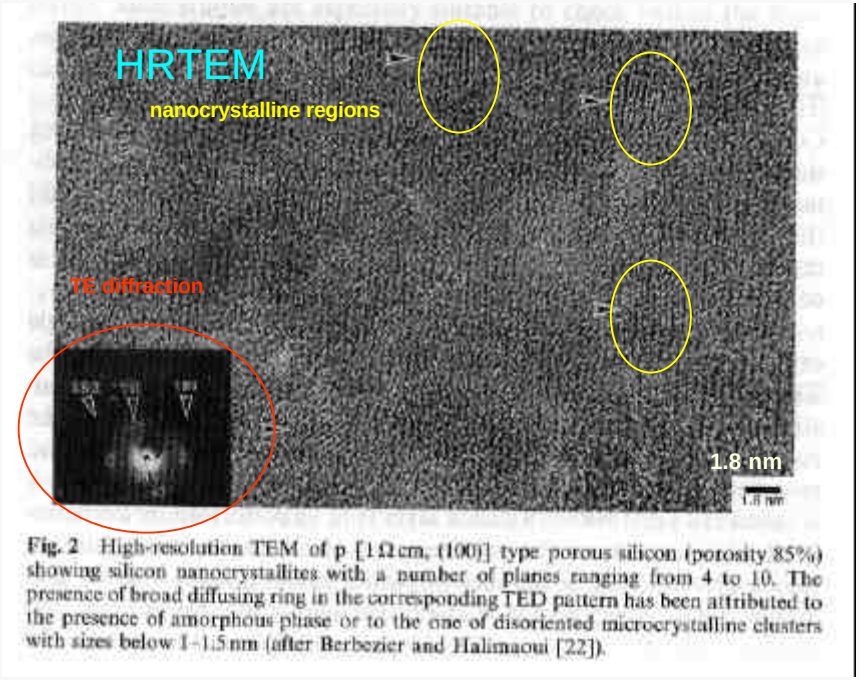

Fig. 2 High-resolution TEM of p [1 Ω cm, (100)] type porous silicon (porosity 85%) showing silicon nanocrystallites with a number of planes ranging from 4 to 10. The presence of broad diffusing ring in the corresponding TED pattern has been attributed to the presence of amorphous phase or to the one of disoriented microcrystalline clusters with sizes below 1–1.5 nm (after Berbezier and Halimaoui [22]).

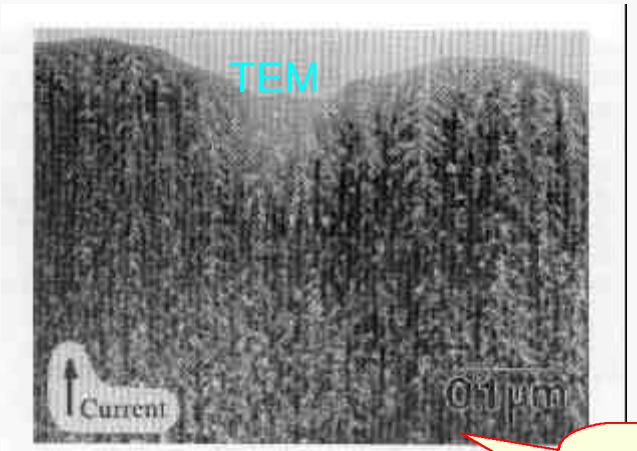

See Amato et al.
Struct. and Opt. Prop. of
Po-Si nanostructures
(Gordon and Breach (1997)

Fotoluminescenza in po-Si

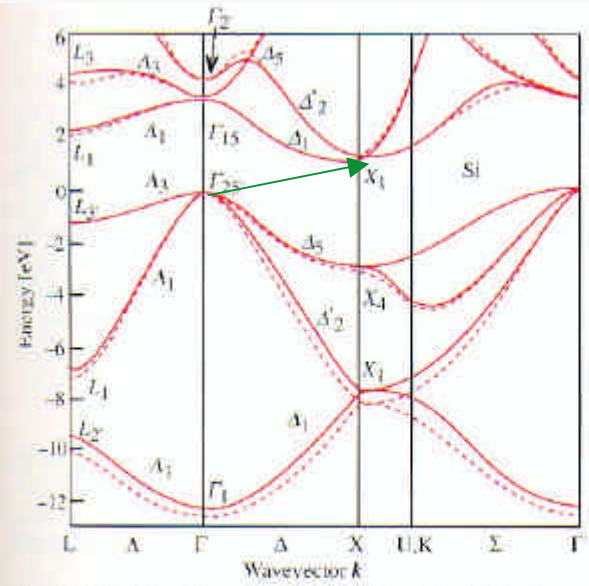

Fig. 2.10. Electronic band structure of Si calculated by the pseudopotential technique. The *solid* and the *dotted lines* represent calculations with a **nonlocal** and a **local pseudopotential**, respectively. [Ref. 2.6, p. 81]

Silicio cristallino:
transizione indiretta
(bassa efficienza)

Da F.F. et al., J. Appl. Phys
91 5405 (2002)

Fotoluminescenza di µ-cavità di po-Si:
analisi SNOM --> aggregati di nanocristalli di Si

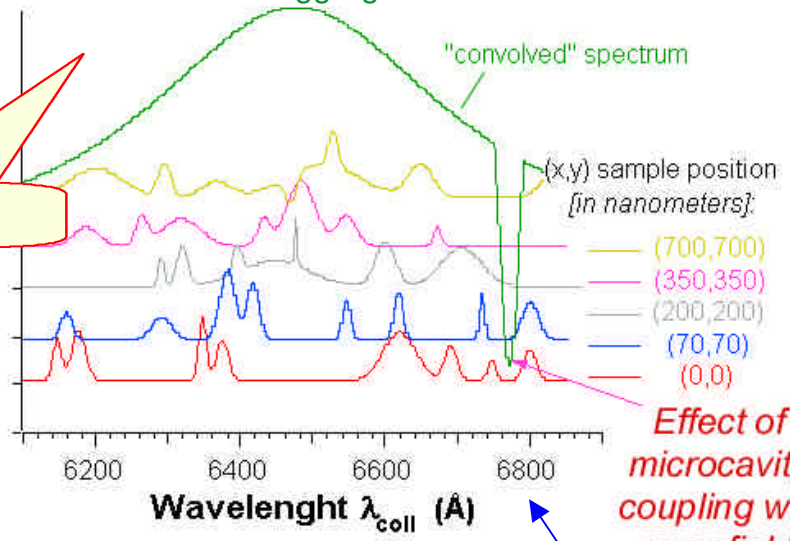

Effect of microcavity coupling with near-field

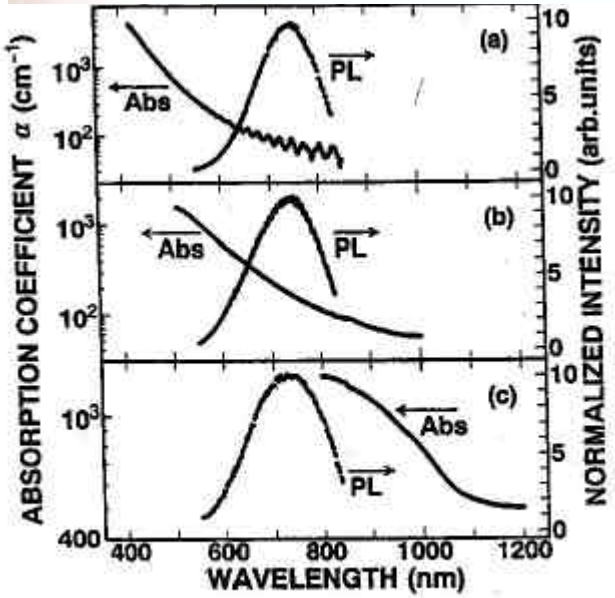

Fig. 1 Typical optical-absorption and photoluminescence spectra of porous Si films: (a) $L \approx 2$ nm, (b) $L \approx 3.5$ nm, and (c) $L \approx 9$ nm. From Ref. [7].

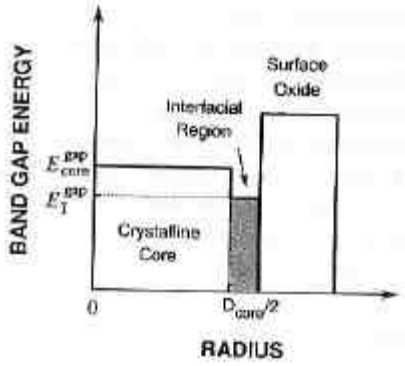

Ruolo porosità (dim. nc-Si)
e passivazione (barriera)
nella PL

Centri emettitori
in LED a Silicio poroso

PL SNOM

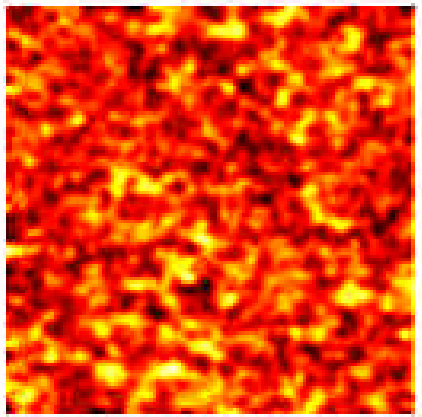

Laser a diodo a eterogiunzione *(tradizionale)*

"Ingredienti" per emissione laser:
- mezzo attivo (guadagno)
- cavità

MQW (eterostruttura)
+ polarizzazione
⇩
eterogiunzione (el. & buche!!)

interfaccia semicond/aria
+ piccole dimensioni (typ. < 1 mm)
⇩
cavità longitudinale

(ulteriore elemento)
definizione laterale cavità
⇩
guida d'onda

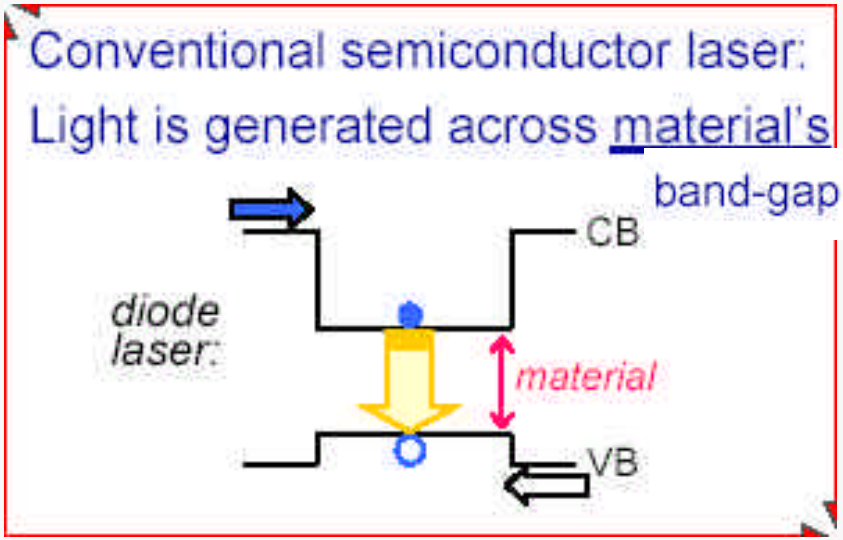

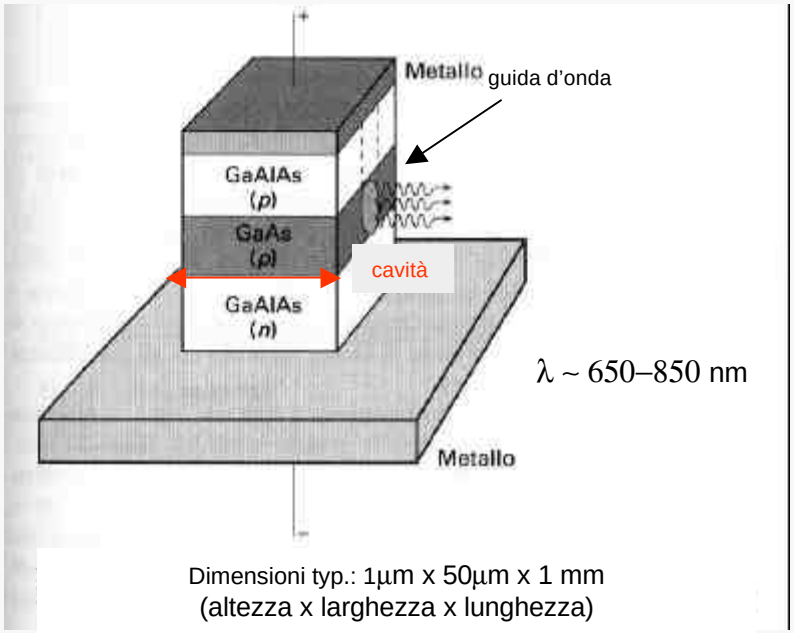

Dimensioni typ.: 1μm x 50μm x 1 mm
(altezza x larghezza x lunghezza)

Emissione legata a ric. eccitoni
(grande guadagno, tunabilità,…)

free spectral range della cavità (piana parallela):
$\Delta\nu = c/2l$

Laser “nanotecnologici” I: quantum dot laser

C.P.Poole F.J.Owens
Introd. to Nanotechnology
(Wiley, 2003)

$\lambda = 1.32\ \mu m$

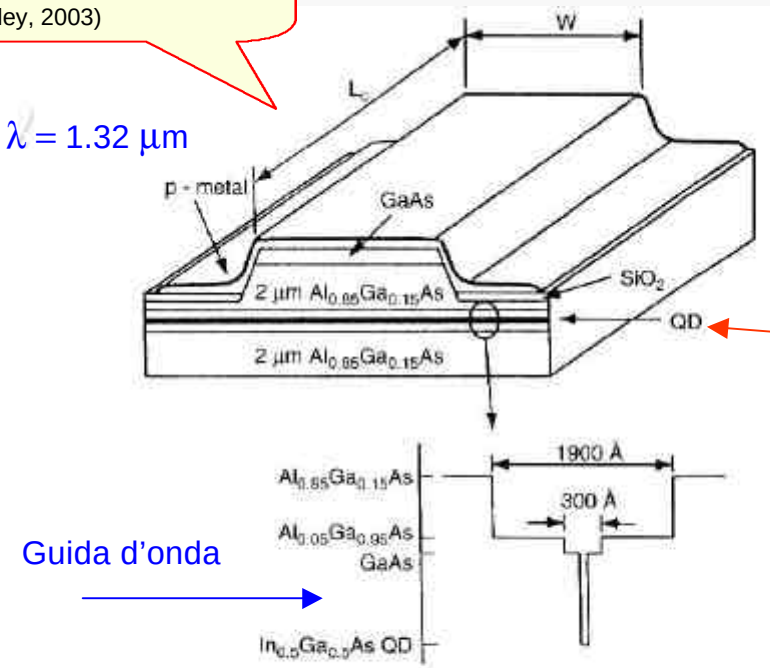

Guida d’onda

Figure 9.24 provides a schematic illustration of a quantum-dot laser diode grown on an n-doped GaAs substrate (not shown). The top p-metal layer has a GaAs contact layer immediately below it. Between this contact layer above and the GaAs substrate (not shown) below the diagram, there are a pair of 2-μm-thick $Al_{0.85}Ga_{0.15}As$ cladding or bounding layers that surround a 190-nm-thick waveguide made of $Al_{0.05}Ga_{0.95}As$. The waveguide plays the role of conducting the emitted light to the exit ports at the edges of the structure. Centered in the waveguide (dark orizontal stripe on the figure labeled QD) is a 30-nm-thick GaAs region, and entered in this region are 12 monolayers of $In_{0.5}Ga_{0.5}As$ quantum dots with a ensity of $1.5 \times 10^{10}/cm^2$. The inset at the bottom of the figure was drawn to epresent the details of the waveguide region. The length L_C and the width W varied omewhat from sample to sample, with L_C = ranging from 1 to 5 mm, and W varying etween 4 and 60 μm. The facets or faces of the laser were coated with ZnSe/MgF_2 igh-reflectivity (>95%) coatings that reflected the light back and forth inside to ugment the stimulated emission. The laser light exited through the lateral edge of ie laser.

Figure 9.24. Schematic illustration of a quantum dot near-infrared laser. The inset at the bottom shows details of the 190-nm-wide ($Al_{0.85}Ga_{0.15}As$ cladded) waveguide region that contains the 12 monolayers of $In_{0.5}Ga_{0.5}As$ quantum dots (indicated by QD) that do the lasing. [From Park et al. (1999).]

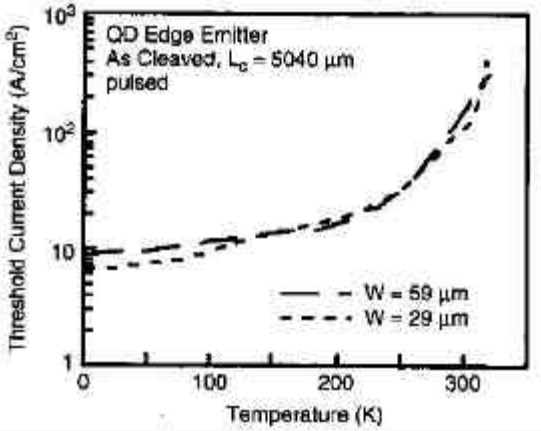

QDs usati per:
- *ottenere λ desiderata*
- aumentare efficienza quantica

⇩

diminuire la corrente di soglia

Effetti non-radiativi (mediati da *fononi*) peggiorano l’efficienza

Laser “nanotecnologici” II: cavità verticale (VCSEL)

Distributed Bragg Reflector structure

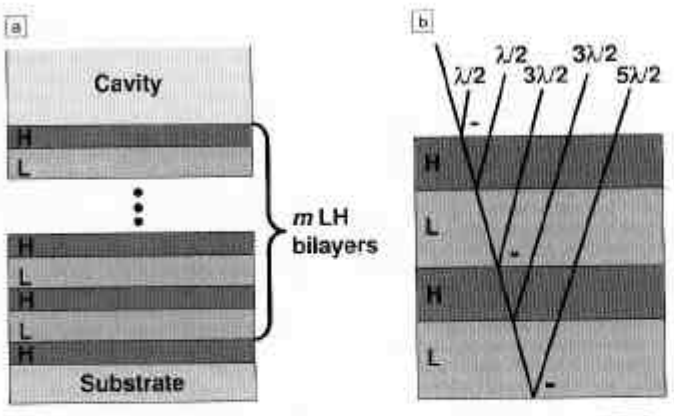

Figure 1. (a) Distributed Bragg reflector (DBR) structure using a high-refractive-index quarter-wave layer on the substrate followed by m low-index/high-index (LH) quarter-wave bilayers. (b) Relative phases at the DBR surface of light rays reflected from each interface within the DBR structure. The minus sign indicates the 180° phase shift that occurs upon reflection from a low- to high-index surface. A round-trip pass through each quarter-wave layer results in a half-wave phase shift. Every reflected ray returns to the DBR surface shifted by exactly 180° in phase. All reflected electric fields thus add constructively to give a high net reflectance for the DBR, even if individual interface reflectances are small.

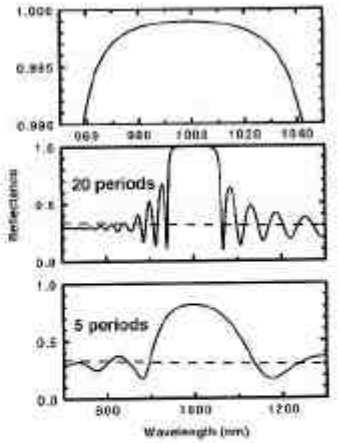

Figure 2. Reflectance spectrum in air of a 1000-nm GaAs/AlAs DBR for 20 periods and 5 periods (lower two plots). Dashed lines show the reflectance from a bare GaAs substrate. Top plot shows the high-reflectance region of the 20-period mirror near the design wavelength.

Possibilità di depositare strati sottili con spessore controllato al monolayer

⇩

fabbricazione di microcavità e “specchi” di Bragg

See MRS Bull. 27 (July 2002)

QD-Vertical Cavity Surface Emitting Laser

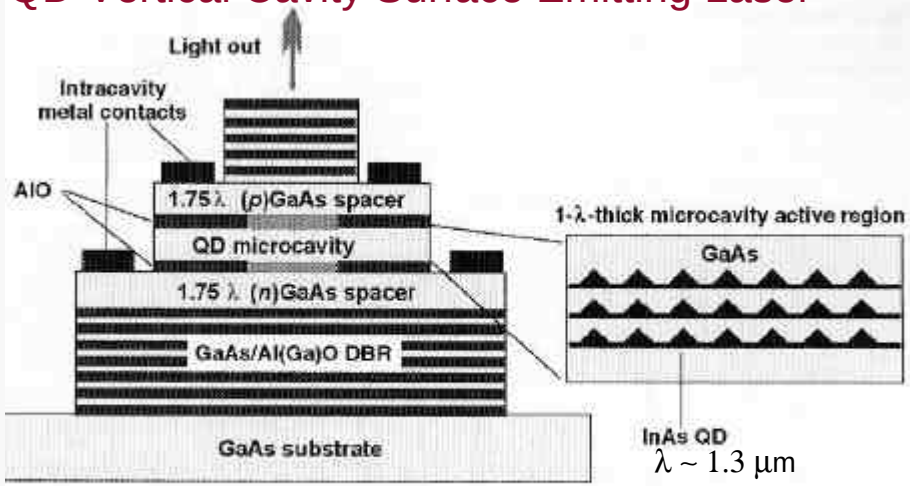

Figure 9. Schematic representation of a QD VCSEL. DBR: distributed Bragg reflector.

Vantaggi VCSEL:

- cavità “corta”: qualità ottica, indipendenza dalla temp., ...
- piccole dimensioni: bassa soglia, efficienza, ...
- emissione superficiale: integrazione, densità, ...

Laser “nanotecnologici” III: cascata quantica (QC)

Obiettivi:

- laser nel medio infrarosso con lunghezza d’onda scelta ad-hoc (es. per analisi tracce)
- altissima efficienza (bassa corrente di soglia, elevata potenza)

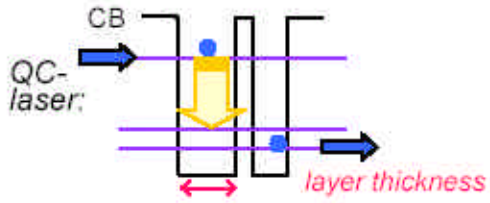

QC-laser:
Light is generated across designed energy gap
“materials by design”:
band structure engineering and MBE

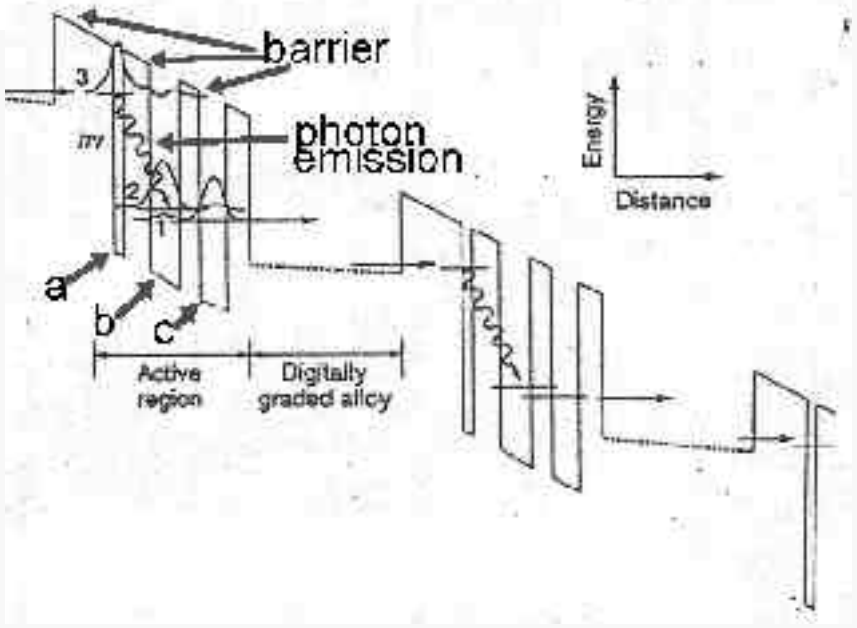

Band-gap engineered attraverso film thickness

Emissione di molti fotoni a cascata

Solo elettroni partecipano (mecc. unipolare)

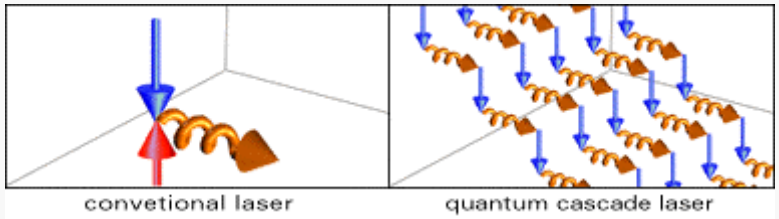

Figure 2

Un elettrone viene iniettato al livello 3 della buca 1, ed emette un fotone decadendo al livello 2 (**il ΔE dipende dallo spessore!!).** Quindi fa tunneling attraverso la stretta barriera verso il livello 2 della buca 2 (il tunneling coinvolge fononi). Il processo di emissione si può allora ripetere in una configurazione “a cascata” **(molti fotoni da un solo elettrone iniettato!!)**

See http://www.unine.ch/phys/meso

Caratteristiche innovative del QC-laser

Quantum design of QC-laser

J. Faist, F. Capasso, C. Sirtori, D. L. Sivco, J. N. Baillargeon, A. L. Hutchinson, S. N. G. Chu, and A. Y. Cho, Appl. Phys. Lett. ***68****, pp. 3680-3682 (1996).*

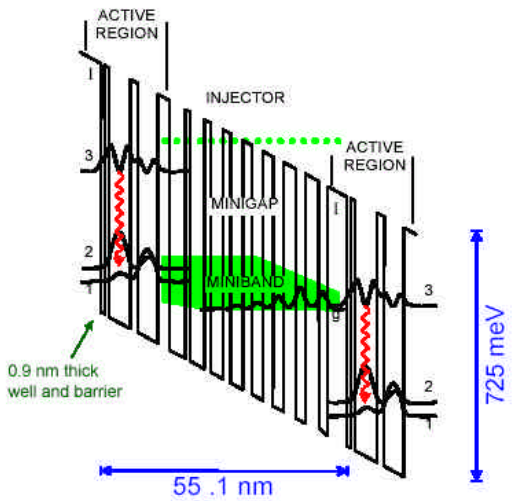

- multiple QWs under external applied electric field
- band-offset = 500 - 800 meV through lattice matched or strain-compensated n InP
- 1 - 100 active regions/injectors (typically ~ 30)
- layer thicknesses designed to provide population inversion
  $\tau_{32} >> \tau_2$
- designed for tunneling transport

Lucent Technologies
Bell Labs Innovations

Key characteristics of QC-lasers

- Wavelength ("color") determined by layer thickness rather than by material composition

➡ all mid-infrared spectrum covered by the same material

- Each electron creates N laser photons in traversing an N-stage cascaded structure (N = 20 - 75)

➡ intrinsically high power lasers

- High reliability: low failure rate, long lifetime and robust fabrication

Room temperature, pulsed, single-mode QC-DFB laser @ $\lambda \sim 4.65\ \mu m$

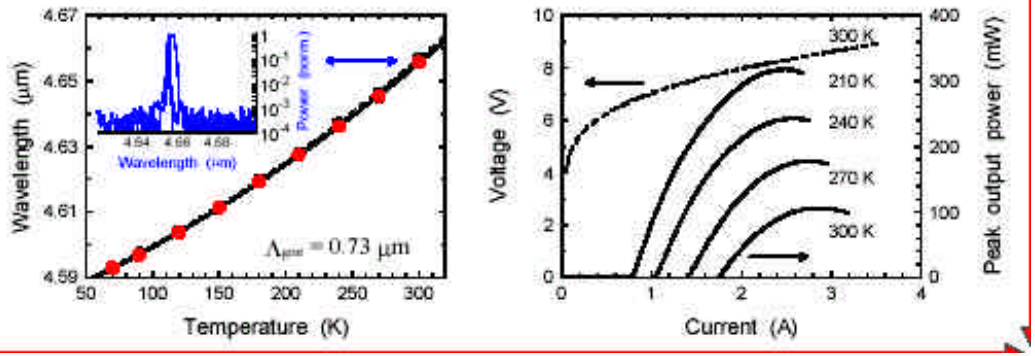

(es.:monitor per tracce di CO)

Wide wavelength-range of QC lasers

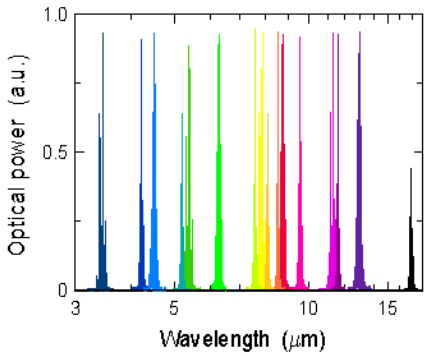

QC lasers cover entire mid-infrared wavelength range (3.4 - 17 μm) by tailoring layer thicknesses of the same material

Fabbricazione di QC-laser

QC-laser crystal grown by Molecular Beam Epitaxy (MBE)

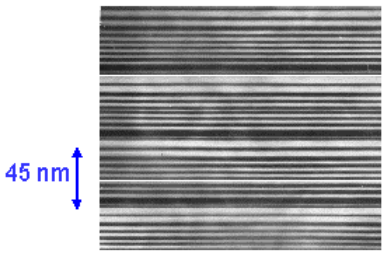

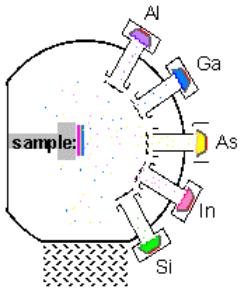

Cross-section of a few stages of QC-laser crystal *crystal growth one atomic layer at a time*

- Many (~ 500), few-atoms thick layers of alloy materials (Al, Ga, As, In);
- atomic control of layer thickness, 1 nanometer (nm) = 4 atomic layers
- atomically flat layer interfaces

Combinazione di MBE (controllo spessori) e litografia (definizione laterale)

TEM / SEM image

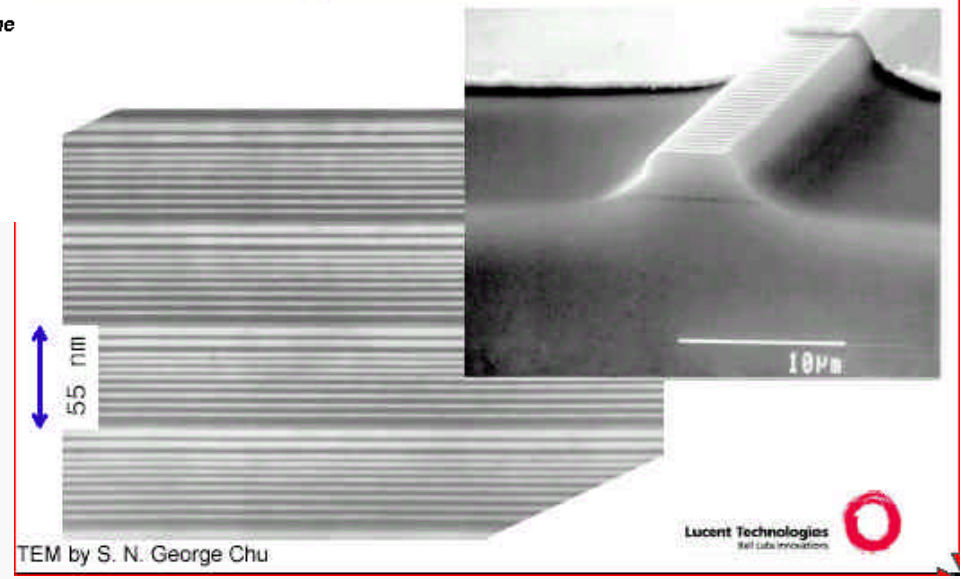

Heterogeneous Cascades (multi-λ generation)

So far:

Homogeneous cascade:

single stack of ~ 30 *identical* active regions & injectors

Now:

Stacked cascades:

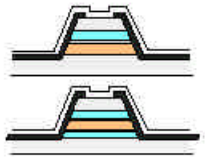

Different electric field across sub-stacks? - OK

Interdigitated cascades:

Charge transport between stages? - OK

Cooperative cascades:

How to design cooperation? see next VGs!

Lucent Technologies

Future possibili implementazioni:
es.: cascata eterogenea

Materiali organici ed optoelettronica

Organic dyes with conjugated π-electron systems have attracted a large and rapidly increasing interest in the last decade as possible materials for various electronic and optoelectronic devices because of their advantageous semiconductor properties. For application as photoactive materials in photocopiers, they have already reached maturity and replaced inorganic semiconductors on a large scale. Efficient electroluminescence (EL) from an organic solid was first demonstrated in large (50 μm to 1 mm thick) single crystals of anthracene [1], [2]. Although these devices showed a high EL quantum efficiency of up to 8 %, they were impractical due to the large applied voltage (>1000 V) required to inject electrons and holes into the crystal. More recently, practical organic light-emitting devices (OLEDs) consisting of sequentially vacuum-deposited layers of hole- and electron-transporting molecular materials [3], [4], [5], [6] or of spin-coated thin polymer films [7], [8] have been demonstrated with active device thicknesses of only a few hundred Ångstroms. Applying about 3 to 5 V, they are already brighter than a conventional TV screen with much higher efficiencies, brilliant colors, large viewing angle, switching times fast enough for video real time image displays and lifetimes well above 10,000 hours. The first displays based on organic semiconductors have become commercially available and companies like Pioneer and Philips and many others are currently developing this promising technology. Small independent firms, such as Universal Display Corporation in the U.S. and Cambridge Display Technology in the U.K., have been created solely to turn these innovations into commercial reality.

The large interest is not only caused by technological aspects such as the low costs, the possibility to prepare flexible large area devices at low process temperatures on polymer foils, and the almost unlimited variety of organic compounds that allow tuning of e.g. energy levels and emission colors. They also have some unique physical properties and advantages compared to inorganic semiconductors [9]. Due to their low dielectric constants, the reflection losses at interfaces are lower than for III-V-semiconductors. The internal fluorescence efficiency is close to unity for some organic dyes with their emission peaks strongly red shifted to the absorption edge thus avoiding re-absorption losses in the devices. For this reason, it is possible to prepare efficient sandwich structures of several OLEDs with different emission wavelengths [10]. The electronic structure of organic semiconductors is largely determined by the individual molecules and only weakly modified by solid state effects. Therefore, interface states play a minor role. Also, amorphous layers grown on cheap, flexible substrates exhibit attractive electrical properties to allow for efficient electroluminescence. The amorphous matrices also enable the incorporation of a wide range of dopants, if necessary in high concentrations, to tune both the conduction type [5], [11] and the emission wavelength [12]. For instance, the admixture of about 7 % of phosphorescent dyes has led to OLEDs that convert 100 % of the electrically excited molecular states into visible light with internal efficiencies close to unity [4], [13], [14].

Figure 15: A flexible 0.18 mm thick passive matrix OLED display fabricated by Universal Display Corporation.

Conducibilità materiali organici
+
emissione ottica da ricombinazione

⇩

diodi emettitori *organici*:
(es.: per large panel displays)

Tecnologie emergenti I: emettitori di luce organici (OLEDs)

in OLEDs light-emitting excitons are formed by the recombination of electrically injected electrons and holes. Therefore, the organic layer system is sandwiched between two electrodes, the work function of which matches the molecular orbital energy levels of the adjacent organic layers (Figure 2). Holes are injected from the anode, which is usually the transparent electrode, consisting of indium tin oxide (ITO). The holes proceed via hopping of defect electrons in the HOMO (highest occupied molecular orbital) energy level of the hole-transporting molecules. Similarly, electrons are injected from the low-work-function cathode and proceed via the LUMO (lowest unoccupied molecular orbital) energy level of the electron-transport layer. From an electrochemical point of view, the charge-transport mechanism can be regarded as mutual solid-state redox reactions involving molecular radical cations for hole transport and radical anions for electron transport, respectively. By recombination, singlet and triplet excited states are formed that emit light directly or undergo excitation-energy transfer. In guest–host systems, however, with dopants acting as charge-carrier traps, recombination predominantly takes place at the dopant.[46]

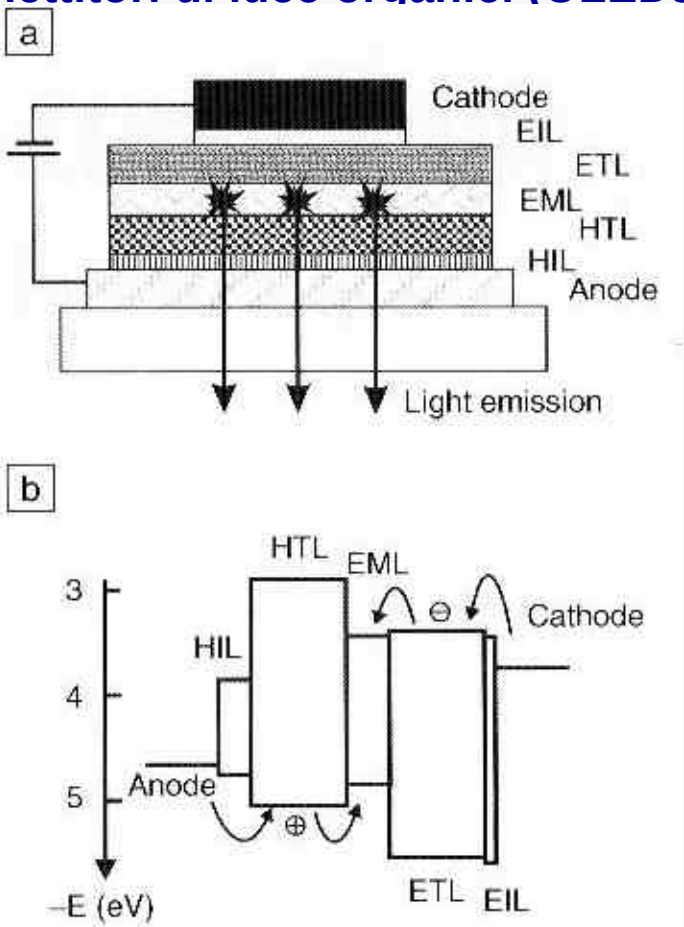

Figure 2. (a) Structure and (b) energy-level diagram of a typical organic light-emitting diode (OLED). EIL = electron-injection layer, ETL = electron-transport layer, EML = emission layer, HTL = hole-transport layer, and HIL = hole-injection layer.

See MRS Bull. 27 (July 2002)

OLED con emissione da polimeri o “assistita” da coloranti (host-guest systems)

Materiali per OLEDs I

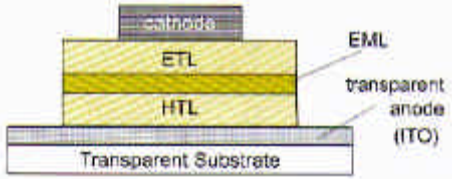

Figure 1: Schematic cross section of an organic light emitting device (OLED) showing the contacts, the electron transport layer (ETL), the light-emitting layer (EML) and hole transport layer (HTL). The total thickness of the organic layers is typically around 100 nm.

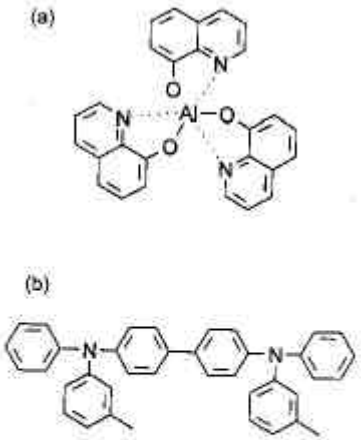

Figure 2: Chemical structures of (a) Alq_3, an electron transport and green fluorescent emitting material and (b) TPD, a hole transport material.

A schematic cross section of a conventional, small molecule based OLED with three organic layers (a double heterostructure) is shown in Figure 1. The top, ohmic, electron-injecting electrode consists of a low work function metal alloy, typically Mg-Ag or Li-Al, deposited by vacuum evaporation. The bottom, hole-injecting electrode is typically a thin film of the transparent semiconductor indium tin oxide (ITO), deposited onto the substrate by sputtering or electron beam evaporation. Light is emitted through this electrode when the device is operated in *forward bias*, i.e., with the ITO biased positive with respect to the top electrode. The next layer deposited is a hole transporting layer (HTL) of a material such as TPD. This is followed by the light emitting (EML) layer consisting of, for example, Alq_3 for green light or a host material doped with fluorescent or phosphorescent dyes and optionally an additional electron transport layer (ETL). The chemical structures of N,N'-diphenyl-N,N'-bis(3-methylphenyl)1-1' biphenyl-4,4' diamine (TPD) and tris (8-hydroxyquinoline) aluminum (Alq_3) are shown in Figure 2. E

[illegible] of organic full color displays.

Organic light emitting devices can be prepared either from **small molecules** (c.f. Section 2.1) or from **polymers**. While the basic physics of both classes of materials is similar, the fabrication processes are very different. Small molecules are usually deposited by thermal evaporation in high or ultrahigh vacuum. Alternatively, the molecules can be evaporated into a stream of a hot inert gas directed to the substrate [17]. This so-called organic vapor phase deposition (OVPD) may provide a means for inexpensive and large-scale manufacturing. The typical sublimation temperatures are between 200 and 400°C. The molecules often have a thermal decomposition temperature much higher than the sublimation temperature. In this case, materials can be purified by repeated sublimation in vacuum or in an inert gas [18]. To separate components with different sublimation temperatures, long glass tubes inside a furnace with a temperature gradient are used. Such high purity materials are not only needed for good device performance, but are essential for long device operational lifetimes. Thermal deposition in vacuum or in the gas phase also allows for easy fabrication of multilayer devices. With sophisticated multilayer architectures, the distribution of charge carriers and excitons can be tuned (cp. e.g. Section 3.2 and 3.3). Small molecular weight devices with long lifetimes have been demonstrated to emit across the visible spectrum [19]. The highest emission efficiencies have been reported for small-molecular weight devices using phosphorescent emitters [13].

Polymers, on the other hand, cannot be deposited or purified by thermal evaporation because their decomposition temperature is generally lower than their sublimation temperature. Devices are accordingly prepared from solution, e.g. by spin coating. A particular advantage of polymers is their adaptability to potentially low cost large-scale display production by ink jet printing [20]. With optimized chemical synthesis and purification procedures, green and blue polymers with high fluorescence efficiencies have been obtained. Green polymeric OLEDs have also reached operational lifetimes in excess of 10,000 h. Polymer devices also have lower operating voltages than devices made from small molecules. However, using controlled doping, small molecular weight devices can compete here as well [5].

Da R. Waser Ed., Nanoelectronics and information technology (Wiley-VCH, 2003)

Polymers
Vs
Small molecules

Metodi fisici di preparazione film sottili

Materiali per OLEDs II

2.1 Isolated Molecules and Molecular van der Waals Crystals

The basic electronic structure of the class of organic molecules typically used for OLEDs is similar to the benzene discussed in Chapter 5. They feature a π–electron system delocalized over the entire molecule and characterized by frontier orbitals know as the HOMO (highest occupied molecular orbital) and LUMO (lowest unoccupied molecular orbital). As discussed below, these two orbitals largely determine the electrical and optical properties of both the single molecules and the molecular solids. The HOMO is a fully occupied bonding π–orbital, and the LUMO is an antibonding unoccupied π^*–orbital. Thus, the π-electron-system is typically saturated (i.e. fully occupied with no upaired spins); hence intermolecular covalent bonds cannot form. Consequently, the solids formed of such molecules are only bonded by weak van der Waals forces [9].

The overlap of the π-electron-system of adjacent molecules is small, leading to an energetic splitting of the order of tens to a few hundred meV. Nevertheless, this splitting is sufficiently large for ordered molecular crystals to show band-like charge transport at low temperatures, i.e. the HOMO levels form a narrow hole transport band and the LUMO levels split into a narrow electron transport band. Note that the overlap of the π–orbitals of neighbouring molecules is generally much smaller than the *intra*molecular overlap of the p_z–orbitals of neighbouring C-atoms inside the individual molecules, leading to the splitting between the different π–electron-orbitals of the molecule. Accordingly, the narrow bands that arise from each of the molecular π–orbitals exhibit only a small *inter*molecular overlap. Such systems are often called *small molecular* systems or *low molecular weight* systems even though the total number of atoms forming such small molecules can be on the order of fifty or more.

The situation is somewhat different in polymeric systems where the large number of C-atoms taking part in the π–conjugation leads to broad quasi-continuous energy bands of π–electron states along the molecular chains. However, this does not imply that polymers have larger charge carrier mobilities than small molecular weight solids because the interchain overlap in polymers tends to be small and mobilities are always limited by the most energetically costly hopping steps – in this case a hop between chains. In fact, the highest mobilities are achieved for highly ordered crystals of small, flat molecules that form closely packed stacks with high *inter*molecular π–electron overlap [21], [22].

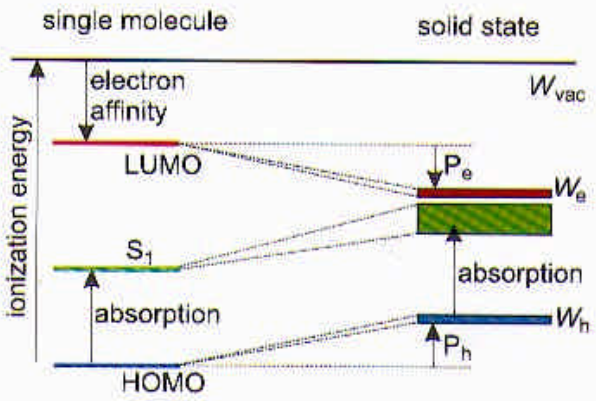

Figure 3: Ionization energy, electron affinity and first optical transition (S_0 to S_1) in a single molecule and formation of charge carrier and exciton bands in molecular solids from the respective molecular orbitals. The ionic energy levels are energetically stabilized in the solid state by the polarization energies P_e and P_h for electrons and holes, respectively. Note that an energetic stabilization of a hole leads to an upward shift in this electron energy picture.

Livelli discreti in “piccole molecole”

Livelli discreti di energia compaiono in sistemi basati su piccole molecole o Van der Waals crystals

Materiali per OLEDs III

In the solid state, the optical gap is 0.5 to 1 eV smaller than the electronic gap [24] due to the Coulomb energy gained when a free electron and hole meet at a molecule to form an excited state or *exciton* [9]. Molecular excitons are different from hydrogenic Wannier-excitons found in inorganic semiconductors. In a molecular *Frenkel exciton* the electron and the hole are localized on the same molecule, typically on the same lig and. In ordered crystals, bands of Frenkel excitons can be formed by wave-type linea combination of molecular excitations, i.e. the exciton may be delocalized even thoug the electron and the hole are coulombically bound. For closely packed materials of fla molecules, the energy of these delocalized states may differ from an excitation on ar individual, *free* molecule by several hundred meV. This leads to the formation of broa exciton bands, and the absorption of the solid differs significantly from single molecule in solution [9]. Accordingly, the excitons couple strongly the phonon system, which ca lead to exciton self-trapping by excimer formation [25]. Here, an excimer is an excite state shared by two, adjacent molecules, causing them to *bind* somewhat more tightl than in their ground state, thus giving rise to a new, lower energy excitation than tha afforded by a simple Frenkel state. Excimers provide additional channels for non-radia tive decay (e.g. aggregate quenching). Therefore, non-planar molecules that form amor phous, loosely packed solids are typically chosen for OLEDs. In this latter case, th optical absorption spectrum is similar in solution and in the solid state since the Frenke exciton is localized on a single molecule. This excitation can diffuse around the solid b hopping transport. For Alq_3, e.g., the exciton lifetime is 16 ns [26], leading to a diffusio length of 10 – 20 nm [26], [27].

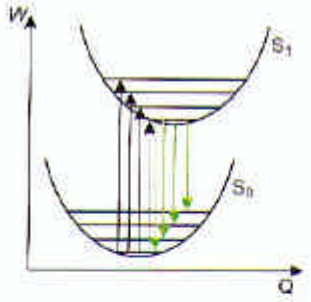

Figure 4: Potential energy lines and vibronic levels for the ground state S_0 and the first excited state S_1 as a function of a configuration coordinate Q reflecting the intramolecular atomic distances. The electronic transitions without change in Q are always most pronounced in the spectra. Clearly, the absorption wavelengths (black) are larger, in general, than the emission wavelengths (green), causing a red shift of the emission spectrum with respect to the absorption spectrum.

Emissione rotovibrazionale (Vs eccitoni nei solidi inorganici)

2.3 Charge Carrier Transport

As in the case of conventional crystalline semiconductors such as Si, perfect molecular crystals show band-like charge carrier transport at low temperatures even though the bands are significantly energetically narrower in organic materials [21]. However, at room temperature, carriers are often localized on individual molecules [21] since the energy bands narrow at higher temperature along with increasing thermally induced molecular vibrations and lattice vibrations (phonons) that reduce the intermolecular π-electron overlap. Eventually, the electron-phonon interaction energies exceed the electronic bandwidth and charge carriers become trapped on individual molecules. In contrast, wider bandwidths exist in conventional semiconductors due to the considerably tighter covalent interatomic bonds. In this case, lattice vibrational energies are much smaller than the electronic bandwidth, significantly reducing the probability of electronic localization (i.e. self trapping) on an individual constituent lattice atom. These effects lead to typical room temperature hopping mobilities of ~1 cm^2/Vs for most organic single crystals, which is two to three orders of magnitude lower than observed for conventional semiconductors. Furthermore, the charge carrier mobility decreases by another four to six orders of magnitude due to structural disorder in amorphous or polycrystalline thin films. Here, a distribution in the trapping energy (the polarization energy) due to the distribution in relative molecular orientations characteristic of disordered solids, leads to a distribution of the energetic density of transport states (DOS) [23]; consequently electron transport can be described by variable-range hopping in the tails of these distributions [28]. In such a situation, the effective mobility increases with the density of injected carriers or the electron donor or acceptor dopant density, respectively: With increasing occupation, the highly localized states deep in the tail of the distribution saturate while states close to the center of the DOS become occupied. Here, the density of states is high, the mean hopping distance is correspondingly reduced, and the hopping rate increases. This leads to a superlinear increase of conductivity with the doping concentration [29] and, for undoped samples, to a current that increases rapidly with the applied voltage [30] (c.f. Section 3.5).

Meccanismi di trasporto delle cariche basati su hopping elettronico

Operazione OLEDs

3.2 Single and Double Layer OLEDs

The operation principle of a single layer OLED is schematically shown in Figure 5. For such devices, the exciton recombination region is near the middle of the device if injection of holes from the anode and electrons from the cathode into the organic material is equally efficient, and the mobilities for both carrier types are also equal. Otherwise the active region where excitons are formed moves close to one of the electrodes which leads to a reduced efficiency: The type of carrier which is more mobile or more efficiently injected has a higher probability of reaching the opposite electrode without being captured by the opposite charge type (thereby reducing γ). Moreover, excitons formed close to an electrode may be quenched by defects or diffuse to the electrode where they non-radiatively recombine.

Typical OLEDs therefore consist of at least two or three layers of different organic materials (c.f. Figure 1), i.e. forming single or multi-heterojunction devices. The single heterojunction device of Tang and van Slyke [3] consisting of TPD and Alq_3 sandwiched between ITO and Al, marked a breakthrough in low voltage, high efficiency device performance. In their OLED, the energy levels were chosen such that there was only a small barrier to hole injection from the hole transport layer (HTL) into the light emission layer (EML), while electrons from the EML met a high barrier so they were not able to penetrate into the HTL. Consequently, there are almost no loss by electrons reaching the anode. On the other hand, the hole mobility in the EML was much lower than the electron mobility. Therefore, the active region is close to the heterointerface in the EML, i.e. roughly in the middle of the OLED structure, thus avoiding the problems encountered in single layer devices (see, for example, Ref. [33]).

Even in the double layer OLED, losses by holes reaching the cathode or by quenching at the cathode can be significant, especially if the thickness of the EML is low, i.e. on the order of the exciton diffusion length. However, thin layers of these low mobility (and hence high resistance) layers are desirable to minimize the operating voltage. Consequently, optimized devices comprise a second heterojunction: An electron transport layer (ETL) is inserted between the EML and the cathode. It should have a wider HOMO-LUMO gap and a larger ionization potential than the EML so that neither excitons nor holes from the EML can penetrate into the ETL [34] (c.f. Figure 5). Therefore, this layer is variously referred to as the hole-blocking or exciton blocking layer (HBL or EBL, respectively). Such heterojunction architectures are self-balancing due to their internal barriers, i.e. they guarantee $\gamma \rightarrow 1$ without requiring either the mobilities or contact injection barriers to be equal.

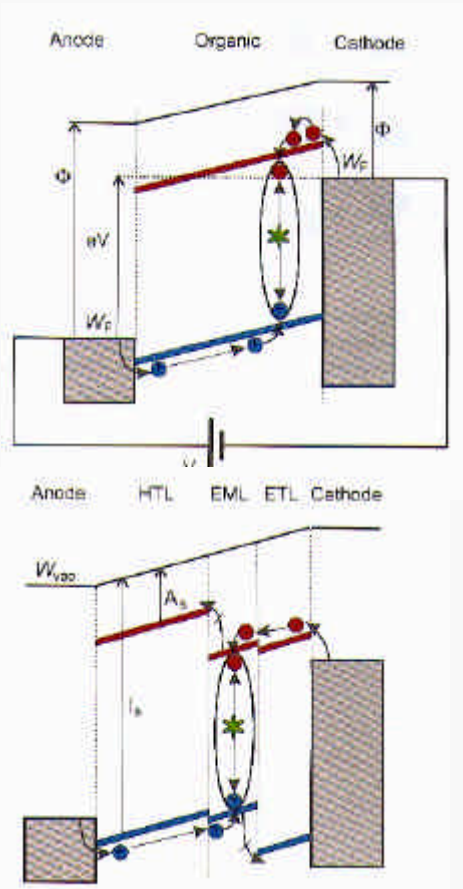

Figure 5: Energy level scheme for a single layer (top) and double heterojunction OLED (bottom) with an applied bias voltage V showing the vacuum energy level W_{vac}, the Fermi levels W_F and workfunctions Φ of the metallic contacts and the hole and electron transport levels of the organic layers. The level offsets at the organic heterojunctions are determined by the different ionization energies I_h and electron affinities A_h of the adjacent layers.

Strutture a doppia barriera “costringono” ricombinazione all’interfaccia e riducono perdite di carica per conduzione tra anodo e catodo

OLEDs con coloranti

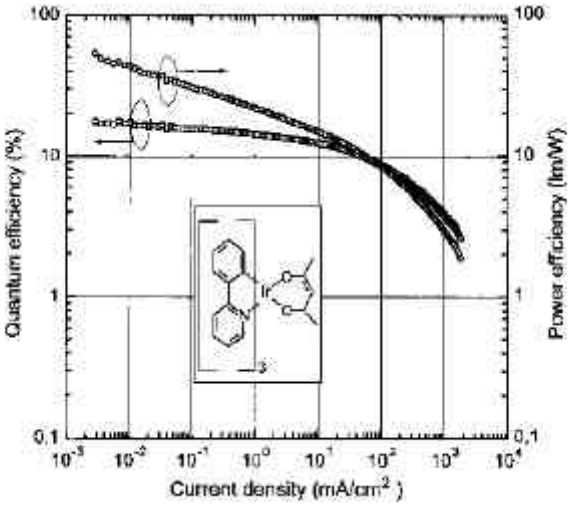

Figure 7: Chemical structure and energy level scheme for the metalorganic phosphor, $Ir(ppy)_3$ (from [38]). The ligand singlet state (^{1}ligand) and metal-to-ligand charge-transfer singlet state ($^1MLCT=S_1$) were determined by the absorption peaks in toluene solution (10^{-5} M). Also, the triplet MLCT state ($^3MLCT=T_1$) was estimated from the phosphorescence peak. κ_{NF}, κ_P, and κ_{NP} are quantum yields for nonemissive transitions from ^{1}MLCT intrinsic phosphorescent transitions, and nonemissive transitions from ^{3}MLCT, respectively. Also, Φ_{ISC} is the yield for intersystem crossing from ^{1}MLCT to ^{3}MLCT.

3.4 High Efficiency Phosphorescent OLEDs

The internal quantum efficiency of fluorescent OLEDs cannot exceed 25 % because of the singlet-triplet-ratio r_{st} discussed above. As shown in Figure 6, there are three ways to form a triplet and only one way to form a singlet. This intrinsic limitation can be overcome by incorporating *phosphorescent guest molecules* into a host matrix material to generate light from both the triplet and the singlet excitons, and achieve internal quantum efficiencies close to unity [13], [14].

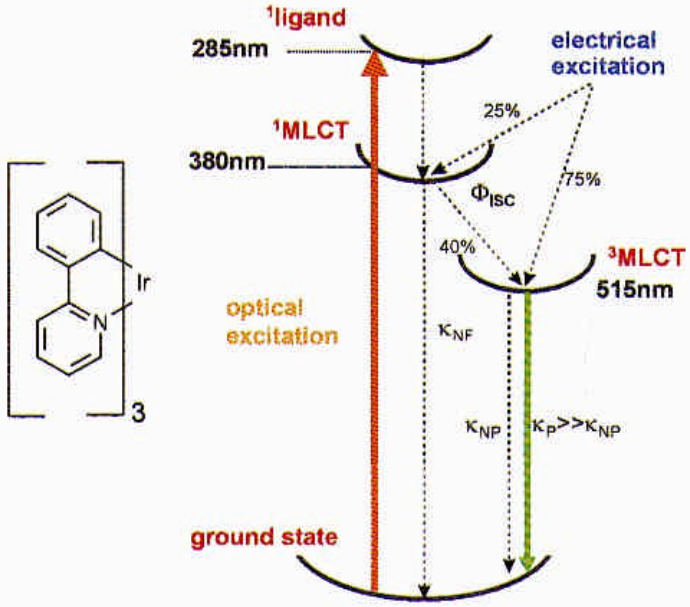

Doping con coloranti aumenta efficienza quantica (singoletto e tripletto eccitati in contemporanea) e permette tunabilità (scelta colore)

Esempi di materiali in OLEDs

Figure 1

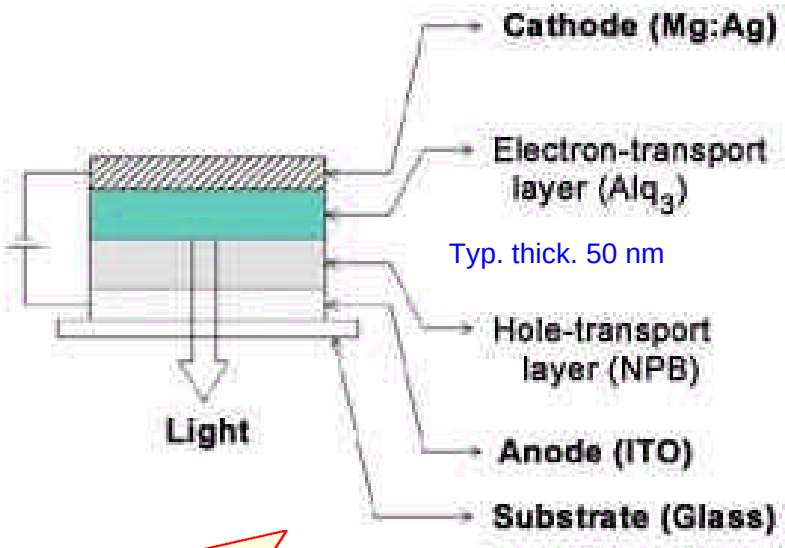

Oemagazine (SPIE, Feb 2001)

Fabbricazione

OLED devices can be divided into two classes: small-molecule devices and organic-polymer devices. Small-molecule devices are fabricated using vacuum evaporation techniques, whereas polymer structures can be applied using spin-casting or even ink-jet printing techniques. Originating at Eastman Kodak Co. (Rochester, NY), the small-molecule technology has achieved commercialization.

Materiali

One of the most basic OLED device structures uses an organic material called NPB as the hole-transport layer and tris-8-hydroxyquinoline aluminum (alq_3) as the electron-transport layer. A typical structure incorporates layers of indium tin oxide/ NPB/alq_3/magnesium-doped silver (ITO/ NPB/alq_3/Mg:Ag), where ITO is the transparent anode and Mg:Ag is the cathode. The energy barriers between the highest occupied molecular orbital (HOMO) and lowest unoccupied molecular orbital (LUMO) levels are about 0.4 and 0.9 eV, respectively, which are sufficiently high to localize the holes in the NPB layer and electrons in the alq_3 layer. Recombination of these charges occurs across the barriers, with holes primarily moving into alq_3. This effect produces excited states or excitons in alq_3 that emit a green fluorescence with its characteristic efficiency. The overall external quantum efficiency is about 1% in photons emitted per charge passing through the OLED device.

Doping

Altering the basic two-layer structure to include a luminescent layer between the hole-transport layer and the electron-transport layer can yield OLED devices with much improved efficiencies. A well-known scheme is to dope the interface region with molecules of high fluorescence efficiencies, as in the three-layer NPB/alq_3:C540/alq_3 structure. Here, alq_3 is the host and C540, a coumarin laser dye, is the dopant present at a concentration of about 1%. The luminescent layer is simply a part of the alq_3 electron-transport layer doped with C540. Because of the enhanced fluorescence from the dopant, the electroluminescence efficiency of the doped OLED device can exceed that of the undoped device by a factor of two to three.

Durata!!

The reliability of OLED devices has been the major concern for practical applications. It has, however, improved substantially over the years. Using various sets of organic materials, many laboratories have reported achieving luminance life (half decay) on the order of 10,000 hours in devices of all colors using various sets of organic materials. Some of the reliability problems, such as the deterioration of the reactive cathode, have been adequately addressed with engineering solutions. The more basic problem of organic material degradation is now better understood. For instance, it has been shown by Zoran Popovic of Xerox Canada, Inc. (Toronto, Ontario) that it is the hole carrier in Alq3 that is partially responsible for the OLED degradation, and remedies for such a degradation include deliberate introduction of stabilizing dopants.

Combinazione OLED + QD

Mobile phones with small colour displays using organic LEDs are already commercially available. The images are generated through fluorescence, as electrons make transitions between orbital states of π-conjugated organic molecules (the π-bond arises from the overlap of the 2*p* orbitals of electrons in carbon atoms). As well as having high quantum efficiency for electron-to-photon conversion, π-conjugated molecules in organic LEDs have the advantage of colour tunability, so that they can be used to build full-colour displays of red–green–blue (RGB) emitters.

But there is also a drawback: the emission spectra of π-conjugated molecules are very broad, typically spanning 50 to 100 nm (the 'full width at half-maximum', or FWHM; Fig. 1, inset). This range of molecular fluorescence is caused by the vibrational and rotational motion of atoms inside the π-conjugated molecules. So with an organic LED, it is difficult to get, for example, pure red light emitted with high quantum efficiency. Nevertheless, sharp RGB emission has been demonstrated from LEDs based on some specific materials, such as europium chelates, aggregated structures of cyanine dyes or layered inorganic–organic perovskite compounds. But these LEDs have not achieved the emission efficiency or device durability needed for practical display applications[2, 3].

Emissione molecolare (es. conj. polymers) è a banda larga!!

Coe et al., Nature 420 800 (2002)

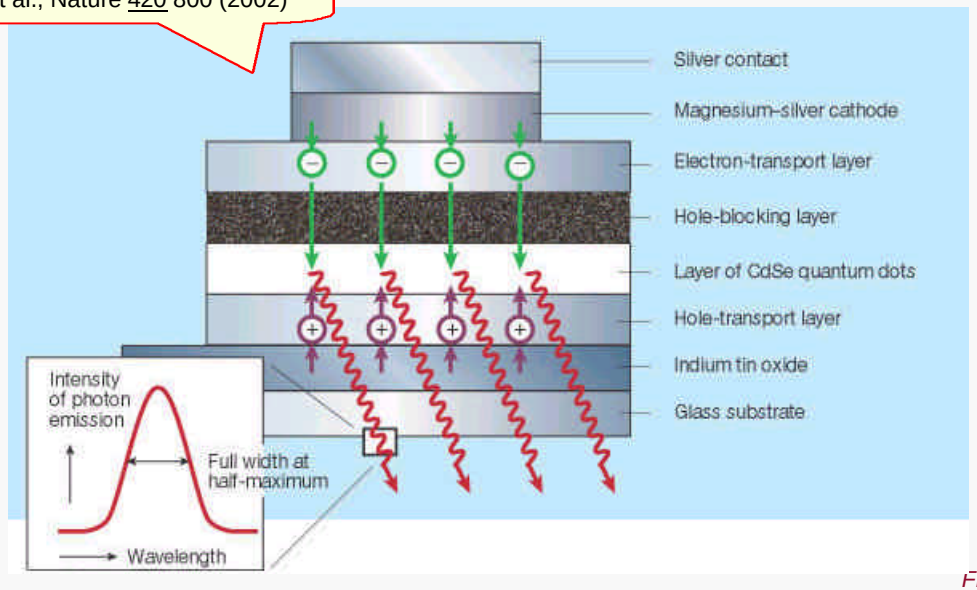

nc-CdSe prodotti da dispersioni in soluzione (tecniche economiche!!)

Doping con nanocristalli di CdSe (QDs) esalta efficienza e restringe banda

Tecnologie emergenti II: cristalli a band gap fotonico (cenni)

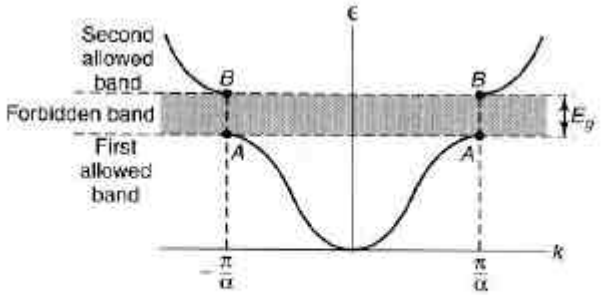

Figure 6.29. Curve of energy E plotted versus wavevector k for a one-dimensional line of atoms.

Richiamo dalla fisica dello stato solido:
per una catena di atomi, la f.ne d'onda elettronica vede un potenziale a bande con un **gap** di energie proibite

C.P.Poole F.J.Owens
Introd. to Nanotechnology
(Wiley, 2003)

important result is that there is an energy gap of width E_g, meaning that there are certain wavelengths or wavevectors that will not propagate in the lattice. This is a result of Bragg reflections. Consider a series of parallel planes in a lattice separated by a distance d containing the atoms of the lattice. The path difference between two waves reflected from adjacent planes is $2d \sin \Theta$, where Θ is the angle of incidence of the wavevector to the planes. If the path difference $2d \sin \Theta$ is a half-wavelength, the reflected waves will destructively interfere, and cannot propagate in the lattice, so there is an energy gap. This is a result of the lattice periodicity and the wave nature of the electrons.

Possibile interpretazione alternativa per il gap:
interferenza (distruttiva) di Bragg (vedi DBR…)

Eq. Schroedinger --> eq. Helmoltz

$$\nabla^2 H(r) + \varepsilon\left[\frac{\omega^2}{c^2}\right] H(r) = 0$$

Onde elettromagnetiche in cristalli artificiali

Equivalent crystal representations:

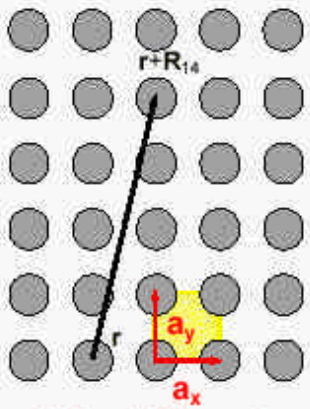

primitive lattice vectors

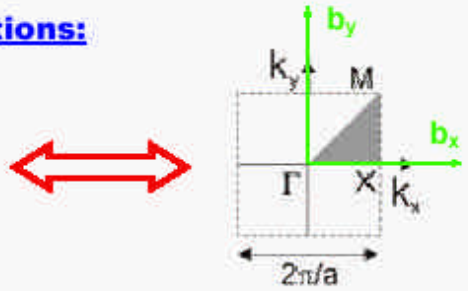

reciprocal lattice
(1st Brillouin zone)

See http://nccr-qp.epfl.ch/qpproject9.htm

$$\varepsilon(\vec{r}) = \varepsilon(\vec{r} + \vec{R}_{mn})$$
$$\vec{R}_{mn} = m \cdot \vec{a}_x + n \cdot \vec{a}_y$$

$$\Phi_k(\vec{r} + \vec{R}_{mn}) = e^{i\vec{k}\cdot\vec{R}_{mn}} \cdot \Phi_k(\vec{r})$$
$$\vec{k} \in 1^{st}\,B.Z.: \left\{\vec{b}_x, \vec{b}_y \,\middle|\, \vec{a}_i \cdot \vec{b}_j = 2\pi \cdot \delta_{ij}\right\}$$
$$\omega_k(\vec{k}) = \omega_k(\vec{k} + G_{pq})$$
$$\vec{G}_{pq} = p \cdot \vec{b}_x + q \cdot \vec{b}_y$$

Photonic Crystals:

Creazione di cristalli artificiali *dielettrici* con band gap in range visibile o near-IR

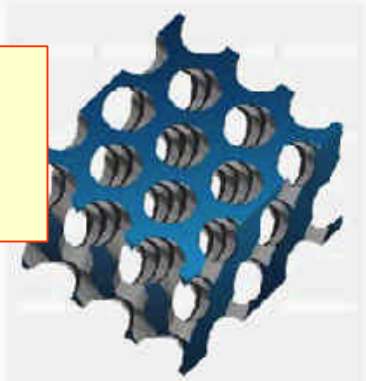

- **Strong periodic perturbation of dielectric material.**
- **Constitutes an artificial dielectric crystal structure → the photonic crysral (PC).**
- **Exhibits wavelength regimes where no propagating solutions are allowed → the photonic bandgap (PBG).**

Spaziature e dimensioni tipiche frazioni di λ (centinaia di nm)

- **Breaking of the crystal symmetry → crystal defects.**
- **Defects: Enable the appearance of localized field states.**

Operazione di cristalli fotonici (pc) I

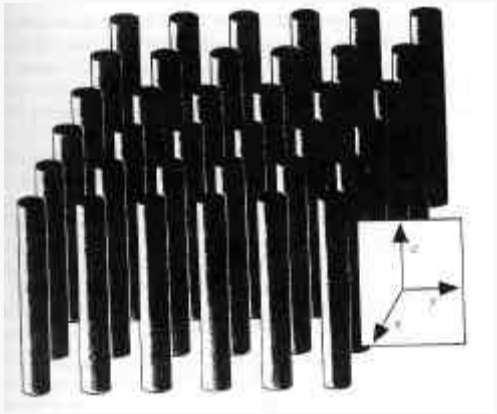

Band gap

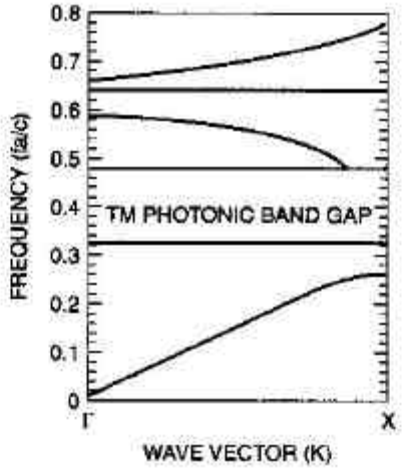

C.P.Poole F.J.Owens
Introd. to Nanotechnology
(Wiley, 2003)

Figure 6.31. A part of the dispersion relationship of a photonic crystal mode, TM, of a photonic crystal made of a square lattice of alumina rods. The ordinate scale is the frequency f multiplied by the lattice parameter a divided by the speed of light c. [Adapted from J. D. Joannopoulos, *Nature* **386**, 143 (1997).]

Esempio di semplice pc 2D
(cilindri dielettrici equispaziati)

Rimuovendo una linea, si rimuove *localmente* il gap

effetto di guida d'onda

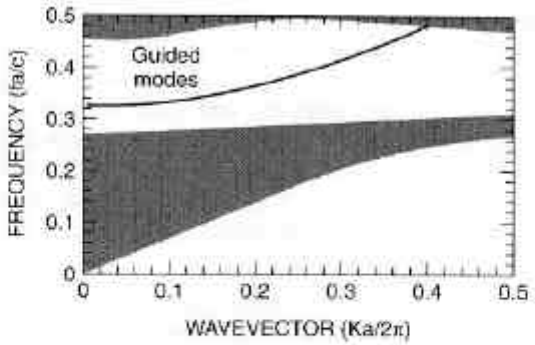

Figure 6.32. Effect of removing one row of rods from a square lattice of a photonic crystal, which introduces a level (guided mode) in the forbidden gap. The ordinate scale is the frequency f multiplied by the lattice parameter a divided by the speed of light c. [Adapted from J. D. Joannopoulos, *Nature* **386**, 143 (1997).]

Guide d'onda (*senza raggio minimo di curvatura*), microcavità, specchi, etc. **integrabili** su dispositivi

Operazione di cristalli fotonici (pc) II

Distribuzione delle perdite per accoppiamento con onde evanescenti investigabile con evanescenti investigabile con SNOM

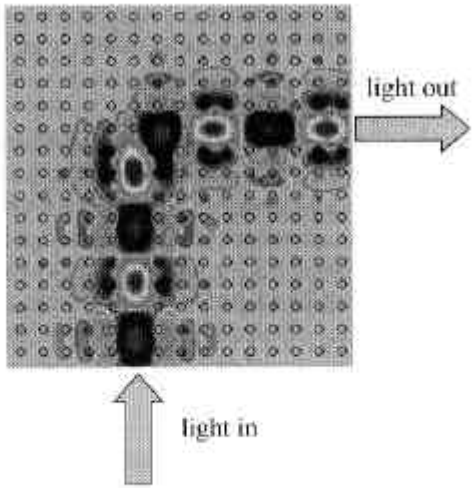

Figure 9.23. Theoretical modeling of field distribution around a defect path way, produc a sharp bend in light propagation. From Mekis et al. (1996), reproduced with permission.

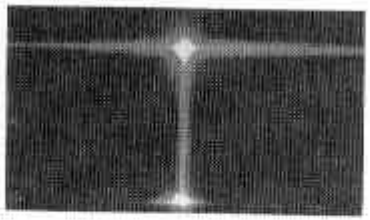

Figure 9.24. A helium–neon laser glows as it enters the waveguide at the bottom and hits the photonic crystal at the top, where it undergoes a sharp bend to propagate in the left and right directions. From Parker and Charlton (2000), reproduced with permission.

"Pieghe" ad angolo retto possibili *senza perdite*

Alcuni esempi di cristalli fotonici I

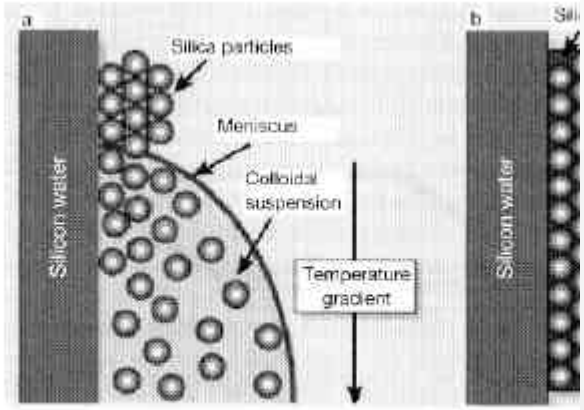

Figure 9.13. Vertical deposition method for crystallization of colloid
duced with permission from Joannopoulos, J. D., *Nature* **414**, 257–258 (

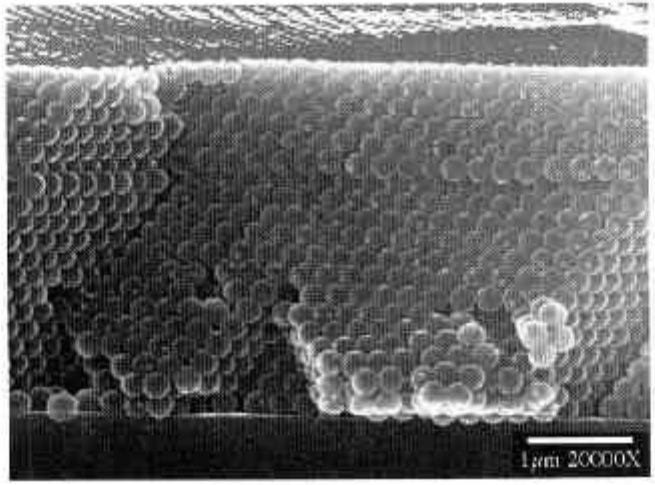

Figure 9.14. Scanning electron microscope (SEM) image of the polystyrene/air photonic crystal, prepared by the vertical deposition method.

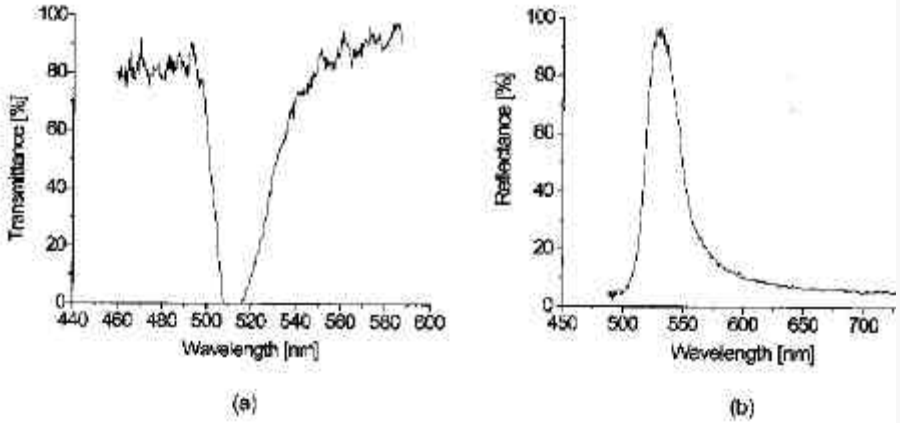

Figure 9.1. Typical transmission (a) and reflection (b) spectra of a photonic crystal p
duced by close-packing of polystyrene spheres. The diameters of the polystyrene spheres
220 nm for transmittance study and 230 nm for reflection measurement.

Possibilità di impiego di tecniche e materiali “speciali” (ma economici)

Alcuni esempi di cristalli fotonici II

See MRS Bull. 26 (Aug 2001)

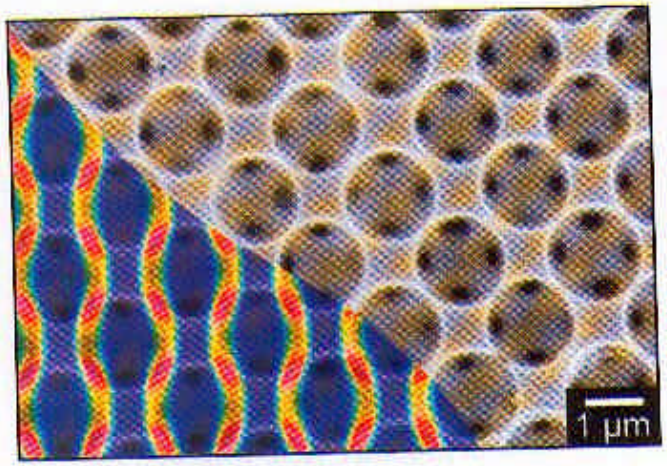

Figure 5. A scanning electron micrograph of a 3D photonic crystal. This structure was assembled by sedimentation of monodisperse colloidal silica on a template, thus forming an fcc structure. Subsequently, molten selenium, which has an index of refraction of 2.5 in the near-infrared and very low absorption, was imbibed into the interstitial space, and the silica was etched away to produce a high-dielectric-constant replica. (From Reference 9.)

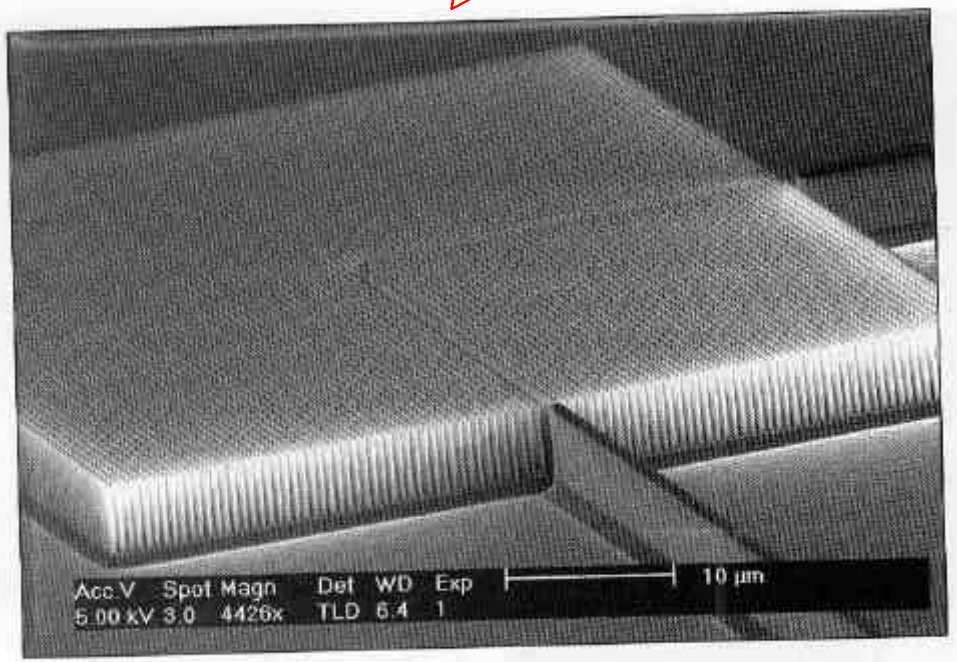

Figure 4. Scanning electron micrograph of a periodic array of silicon pillars fabricated using deep anisotropic etching. The silicon pillars are 205 nm in diameter and 5 μm tall. This structure possesses a bandgap of around 1.5 μm for transverse magnetic polarization. By removing an array of pillars, a waveguide bend may be fabricated. Input and output waveguides are integrated with the photonic crystal.

Micro e nanofabbricazione
per dispositivi integrati in campo ottico,
optoelettronico e **fotonico**

Problema aperto:
dimensionalità > 2